RRS *Charles Darwin* Cruise CD87

Cruise Report

Multibeam Bathymetric and Potential Field Studies of the Reykjanes Ridge

16 June - 20 July 1994

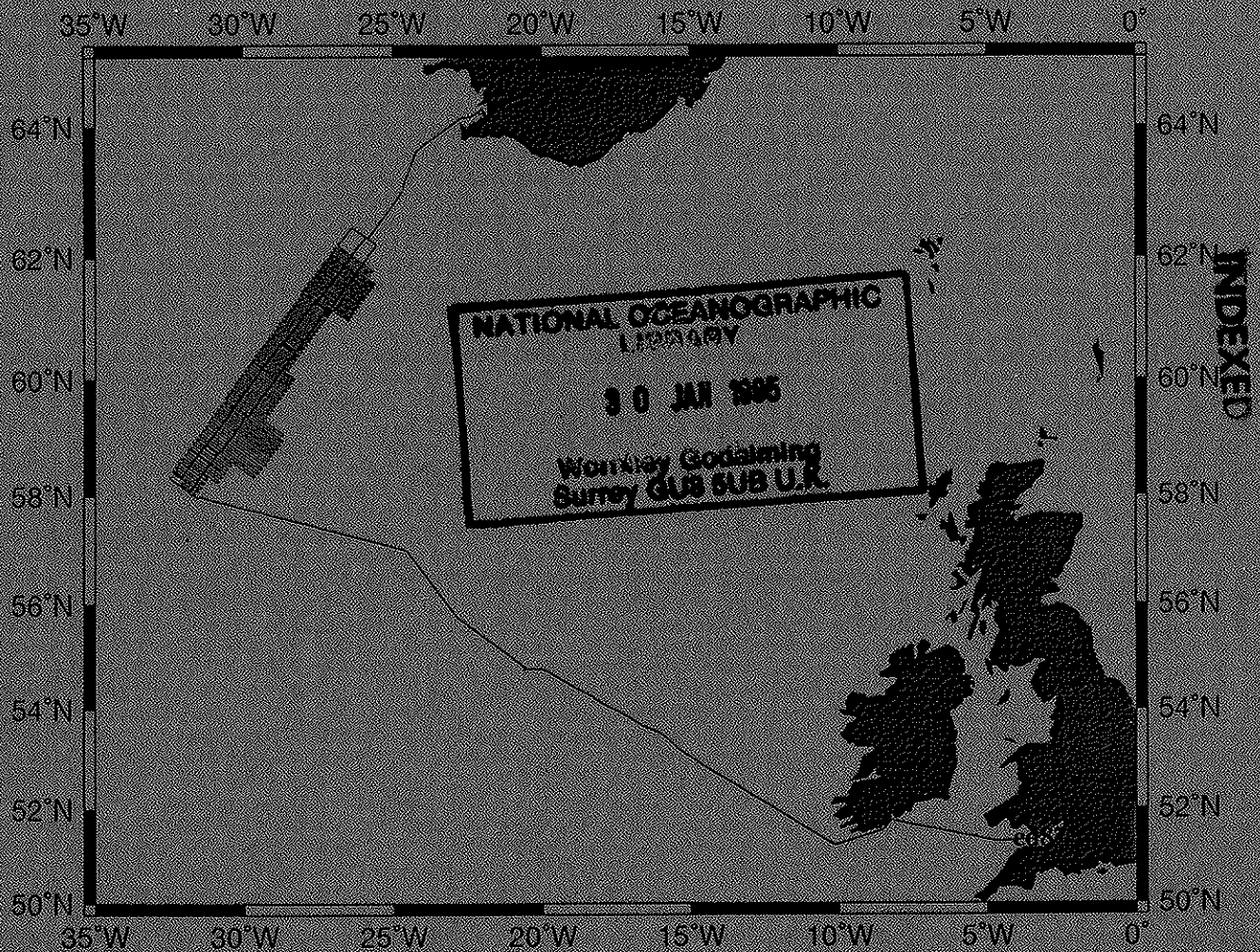

Department of Geological Sciences
University of Durham

CONTENTS

LIST OF FIGURES

1. BACKGROUND

The Reykjanes Ridge is one of the best examples of a hotspot-dominated mid-ocean ridge, and as such has been chosen by BRIDGE as the setting for one of its four regional projects. It has a number of unusual characteristics that are thought to be related to the proximity of the Iceland hotspot and mantle plume (e.g. Vogt, 1971; Courtney & White, 1986; Watson & McKenzie, 1991).

This cruise was funded by BRIDGE from a proposal on which R. C. Searle, B. E. Parsons and R.S. White were co-PIs.

1.1 Gross morphology

The ridge extends along an azimuth of 216° from the Reykjanes Peninsular of southwest Iceland to the Bight Fracture Zone at 57°N, a distance of 900 km, and is spreading at a half-rate of about 12 mm a^{-1} along 090° (Talwani et al., 1971; DeMets et al., 1989). The axial depth increases gradually from the 500 m at the insular margin to about 2000 m at the Bight Fracture Zone. Along the whole of its 900 km length the ridge has no transform faults or large non-transform offsets, and is thus spreading 36° obliquely. The onset of this phase of oblique spreading was slightly diachronous, beginning in the lower Miocene in the north and the middle to upper Miocene in the south (Vogt & Avery, 1974). Prior to that the ridge had many small-offset transform faults that are well-displayed in the magnetic (Vogt & Avery, 1974) and gravity fields (Haxby, 1987; Strange, 1991).

In the north the Ridge is morphologically more akin to a fast- than a slow-spreading ridge, having an elevated axial region rather than a median valley (Talwani et al., 1971). It also has low amplitude axis-parallel fault scarps, producing a regionally smoother seafloor than is found elsewhere in the north Atlantic (Searle & Laughton, 1981). This may be because the presence of anomalously hot mantle and high quantities of partial melt associated with the plume provide a thermal structure akin to that of a fast spreading ridge (Searle & Laughton, 1981; Brozena & White, 1990). The axial high gives way to a shallow median valley south of about 59.5°N.

High mantle temperatures associated with the Iceland plume appear to extend beyond Iceland and give rise to thickened oceanic crust near the Reykjanes Ridge, at least north of 59°N (see below). This partly explains the unusual elevation of the Ridge, although Strange (1991) has shown, using geoid and depth variations to estimate crustal thickness and temperature variations along the ridge, that the inferred crustal thicknesses are smaller than would be predicted for the inferred temperatures using the melting relationships of McKenzie and Bickle (1988).

Vogt & Johnson (1975) demonstrated the existence of SW-pointing V-shaped pairs of ridges with narrow apices. They are associated with strong gravity anomalies and are clearly a major feature of the Ridge. Vogt & Johnson suggested that these ridges represent the trails of volumes of excess melt migrating along the ridge away from the plume (Vogt, 1971). However, White (1992a) has questioned the possibility of such

axial flow. Searle & Laughton (1981) found no disruption of the seafloor tectonic fabric or other morphological feature associated with these ridges, and the origin of the ridges is still uncertain.

1.2 Crustal thickness and density

Seismic studies of deep crustal structure near the ridge axis have been concentrated between 59°N and 63°N. Near 60°N, Bunch & Kennett (1980) ran three axis-parallel lines between the axis and 9 Ma crust. Around 62°N there have been a number of studies. Talwani et al. (1971) made a number of refraction lines using sonobuoys, but did not reach mantle. Snoek & Goldflam (1978) interpreted a line about 2 Ma (20 km) northeast of the axis at 63°N, while Angenheister et al. (1980), Goldflam et al. (1980) and Ritzert & Jacoby (1985) reported on the southernmost axis-parallel RRSIP line over 12-15 Ma-old crust on the southeast flank of the ridge. These studies show 10-km-thick oceanic crust (about 3 km thicker than normal oceanic crust, though still less thick than under Iceland), and some anomalous transitional and mantle structure under the active spreading centre. Crustal thickness measurements from elsewhere in the northern Atlantic also show increased crustal thickness of 9-10 km due to the presence of the Iceland plume (White, 1992b; White et al., 1992).

Recently, White (1992c) has conducted wide-angle and normal-incidence multi-channel seismic experiments on zero-age and 3 Ma lithosphere at 62°N (cruise CD70). Dr. M. Sinha (Cambridge) and Dr. C. Peirce (Durham) shot a further set of wide-angle seismic profiles along and across the ridge axis at 58°N in October 1993 (cruise CD81).

Owens et al. (1991) and Searle et al. (1992, 1994) data suggest the existence of a 10 km, second-order (non-transform) ridge offset at 58°N from bathymetry information and the inversion of the gravity and magnetics data from cruise EW9008, indicating thinning of the crust and magnetic layer and probably cooling of the mantle. This is the only ridge offset (apart from the ubiquitous en-echelon overlaps of AVRs) so far recognised along the Reykjanes Ridge.

Along the axis away from the 58°N offset, the residual Bouguer anomaly gets rapidly more negative, suggesting the existence of the same kind of crust/mantle segmentation as has been found in gravity and topography elsewhere along the Mid-Atlantic Ridge (Kuo & Forsyth, 1988; Lin et al., 1990). However, Bell & Buck (1992), analysing a single along-axis and widely-spaced cross-axis gravity profiles from Talwani et al. (1971) north of 60°N, suggest that the amplitude and wavelength of such segmentation are less than on other parts of the MAR, and interpret this to indicate that raised temperatures allow both a lower degree of segmentation in mantle upwelling (Parmentier & Phipps Morgan, 1990) and ductile flow in the lower crust to compensate partially for the initial crustal thickness variations induced by such segmentation.

1.3 Fine morphology

Following the early geophysical studies by Talwani et al. (1971), a relatively detailed study of the morphology of the Reykjanes Ridge crest between 58°N and 61°N was

carried out by Searle & Laughton (1981) using GLORIA and other sonar. They found that the axial region of the Ridge is characterised by a succession of en echelon axial volcanic ridges (AVRs). The GLORIA survey showed that, as elsewhere on the mid-ocean ridge, major normal faults are formed a few kilometres off-axis. These faults are, unusually, approximately parallel to the ridge axis and oblique to the spreading direction. The horizontal fault pattern appeared to be constant across the axial-high/median-valley boundary, but fault throws changed gradually across it. Similar AVRs and oblique normal faults were mapped at 62°N by Jacoby (1980) using a narrow-beam echosounder.

Hydrosweep multibeam and SeaMARC II bathymetry work (cruises EW9004 and EW9008) confirmed that en echelon AVRs are ubiquitous along the ridge axis, although their size and 'robustness' vary, not monotonically, along it (Appelgate and Shor, 1994; Parson et al., 1993). Parson et al. (1993) and Murton and Parson (1993) have analysed an 'axial profile' based on these data, and suggest that a number of scales of topographic segmentation can be recognised, which they attempt to relate to mantle melting and crustal magmatic processes. In particular they show that the area around 60°N sits on a 'knee' in the axial profile, whose gradient steepens substantially south of there. Moreover, there is at 60°N a robust axial high that comprises many well-developed AVRs. The reason for this local development is not yet known.

TOBI high resolution sidescan data gathered on cruise EW9008 show the AVRs to be of recent volcanic constructional origin, being composed of numerous small, point-source volcanoes, often aligned along what are taken to be buried fissures striking normal to the spreading direction. The AVRs show variable overall levels of acoustic backscattering and are affected by varying degrees of tectonism. These observations suggest variations in age, and have allowed an evolutionary sequence to be suggested (Parson et al., 1993; Murton and Parson, 1993).

1.4 Geochemistry

Schilling et al. (1983) have summarised geochemical results from a detailed sampling programme along the ridge, which allow the influence of the Icelandic plume to be followed in detail. The cut-off for a plume-related geochemical signal appears to be just south of 60°N. Murton et al. (1993) increased Schilling et al.'s sampling density by a factor of ten, with sample stations 2 km or less apart.

1.5 Hydrothermal activity

At present the only known vent field (Steinahóll) on the Reykjanes Ridge is in very shallow water on the Icelandic shelf near 63.1°N (Olafsson et al., 1991). Russian submersible dives took place near 58°25'N and reported hydrothermal staining (Kuznetsov et al. 1985). The US Navy's nuclear submersible NR1 dived near 61.8°N (Uchupi et al, unpublished data), and it is anecdotally reported that Bruce Heezen observed hydrothermal vents during that dive. However, no confirmation or documentary evidence of this can be found. German et al. (1993) sampled every 5 nautical miles along the Reykjanes Ridge, but found no vent sites in addition to Steinahóll.

2. OBJECTIVES

[The following is an extract from the ship-time proposal:]

1. Completion of a detailed multibeam bathymetry, gravity and magnetic survey of the Reykjanes Ridge, as a basis for further BRIDGE activities
If properly integrated with existing surveys, it will be possible to complete a near 100% bathymetric coverage together with closely-spaced magnetic and gravity profiles, extending at least 30 km off-axis on either side, over almost the whole ridge length. This off-axis coverage is sufficient to span the whole width of the AVR zone and will include magnetic anomaly 2 (2 Ma). We will publish the results in map form to assist in future work.

2. Production of bathymetric, gravity and magnetic databases for use in further BRIDGE activities
Our results will be combined with other existing data, particularly those from the 1990 Ewing cruises, and Seasat, Geosat and ERS-1 gravity to produce comprehensive digital databases of the area. Appropriate corrections will be applied to minimise navigation and cross-over errors. These digital databases will be made available to the BRIDGE community for the planning and interpretation of future work.

3. Completion of a sufficiently large and dense bathymetric, gravity and magnetic survey near 62°N to facilitate comprehensive analysis of the CD70 multichannel seismic experiment
We shall extend our coverage over a 100-km-long section near 62°N to 60 km off-axis to the SE, in order to include the whole area of the CD70 seismic survey. The aim is to enable modelling of the acoustic reverberations from seafloor topography, to use gravity to assist in modelling of crustal structure along the seismic lines and, most importantly, to provide the data to compare reflections from within the crust with surface topographic structure.

4. Investigation of crustal thickness variations along the Reykjanes Ridge axis
Four major seismic refraction experiments have been completed along the Reykjanes Ridge spreading axis, which will provide firm control on crustal thickness at 58°N, 60°N, 62°N and 64°N. All will have been modelled with modern synthetic seismogram methods. We shall use the continuous gravity and bathymetry measurements from this cruise to interpolate between these fixed tie points, which will allow us to construct a map of crustal thickness variations along the ridge axis. On a large scale, this will enable us to test convection models of the flow of abnormally hot mantle material brought to the base of the lithosphere by mantle plumes (e.g. Courtney & White, 1986; Watson & McKenzie, 1991) and will provide constraints on melt productivity from the Iceland plume (e.g. White, 1992a). On a smaller scale, it will allow us to map crustal thickness variations on a segment scale to test theories of melt distribution with lateral position at a crustal level.

5. Determination of complete pattern of segmentation and variability of magma supply along the Reykjanes Ridge

Ridge segmentation is now well-recognised on the Mid-Atlantic Ridge and East-Pacific Rise, and is recognised in topography, tectonic and volcanic patterns, and crustal thickness variations. Most of these can and have been related to variations in magma supply. There are many theoretical reasons why one would expect variability in melt migration (e.g. Scott and Stevenson, 1986), and it may well be that the segmentation observed at slow-and fast-spreading ridges reflects this variability. However, at the Reykjanes Ridge the expression of the variability may be different, and we will examine this. Topography, gravity and magnetics will be analysed to determine the current pattern of crustal segmentation along the ridge. We will determine the range of lengths of segments and their offsets, and compare these with data from other ridge areas and spreading rates. Particular attention will be paid to latitudinal variations and their comparison with geochemical anomalies, to try to determine the degree of influence of the plume. We will further test the possibility of a hierarchical segmentation pattern as proposed by Parson et al. (1993).

6. Relationship of near-ridge variations to off-ridge features

Having determined the pattern of axial segmentation and other variations, we will trace these features off-axis where possible or, if there are no continuous off-axis traces, compare previous variation patterns along particular isochrons. We will attempt to compare any pattern found with that of the pre-Miocene transforms, although we realise that such a comparison really requires continuous high-resolution data connecting the two areas, and is properly the subject for a separate study. Spreading rate variations and ridge jumps or propagations will be determined along the whole ridge length. We will examine the relationship between topographic, gravity and magnetic evidence for segmentation, and here too examine the influence of the Iceland plume on these features.

7. Investigation of the structure and origin of the V-shaped ridge pairs

We aim to determine the crustal density/thickness and magnetisation, the degree and means of compensation, and the age/position of formation of the V-shaped ridges. We will also attempt to determine whether the patterns of volcanism and tectonism are different from those on the surrounding seafloor.

8. The origin of axial valleys on normal slow-spreading ridges

Since the Reykjanes Ridge cross-section changes from axial high to median valley, we can use the observed variations in the gravity field along the Ridge to investigate this. We would, for example, investigate the effects of sub-surface loading by magma chambers, and the degree of isostatic or dynamic support of axial high or median valley. We will also investigate changes in faulting across the transition, which will reflect the brittle response to the underlying topographic forcing function.

3. WORK COMPLETED

The ship track is presented in figure 1. It was planned according to the above objectives and used satellite gravity data (Hwang et al., 1994) as a guide (figure 2). The satellite gravity was validated by the ship gravity and appeared to have good resolution down to 10-15 km wavelengths. We nominally divided the survey into five areas: D, E, F, G and H (following on from areas A, B and C of cruise EW9008 - Parson et al., 1993). These are indicated on figure 1 and are referred to in the sections below. Simrad EM12S-120 multibeam bathymetry, LaCoste-Romberg and Bell BGM3 gravity and total field magnetic data were recorded. Figure 3 displays the CD87 ship track together with other cruise tracks which collected similar data.

4. CRUISE NARRATIVE

(All times GMT)

Thur June 16 1994 (Julian Day 167)

0910:	Departed Barry, set passage for Edoras Bank via Cork (for personnel transfer) and Fastnet.
1230:	First science meeting with science party and RVS technicians.

Fri June 17 (168)

0800:	Briefing meeting with Principal Scientist, Master, Chief Officer, Chief Engineer.
0917:	Switched on EM12S-120 for testing and practising operating and processing procedures.
1230:	Science briefing for crew. Making 11 knots on passage.

Sat June 18 (169)

0100:	Ship's clocks to GMT.
0600:	Wind freshening, force 6.
1500:	Full gale. Ship slowing.
1700:	EM12 records very poor - switched off.
2030:	Wind abating. EM12 back on.

Sun June 19 (170)

0940:	A/c for E-W run over Lorien Bank to calibrate EM12.
1100:	Hove to for velocity profile.
1122:	Began velocity dip no. 1, to 2000m.
1300:	Ended velocity dip.
1334:	Launched magnetometer. Begin slow turn to E to start EM12 pitch/roll calibration.
1503:	Commenced daily XBT deployments (see appendix A4).
1822:	End of EM12 calibration. S/c 306° for start of Edoras Bank line.

Mon June 20 (171)

0338:	A/c 323° at start of Edoras Bank line; running over Cambridge seismic line CAM77.
1200:	End of CAM77. A/c 285° for Reykjanes Ridge.

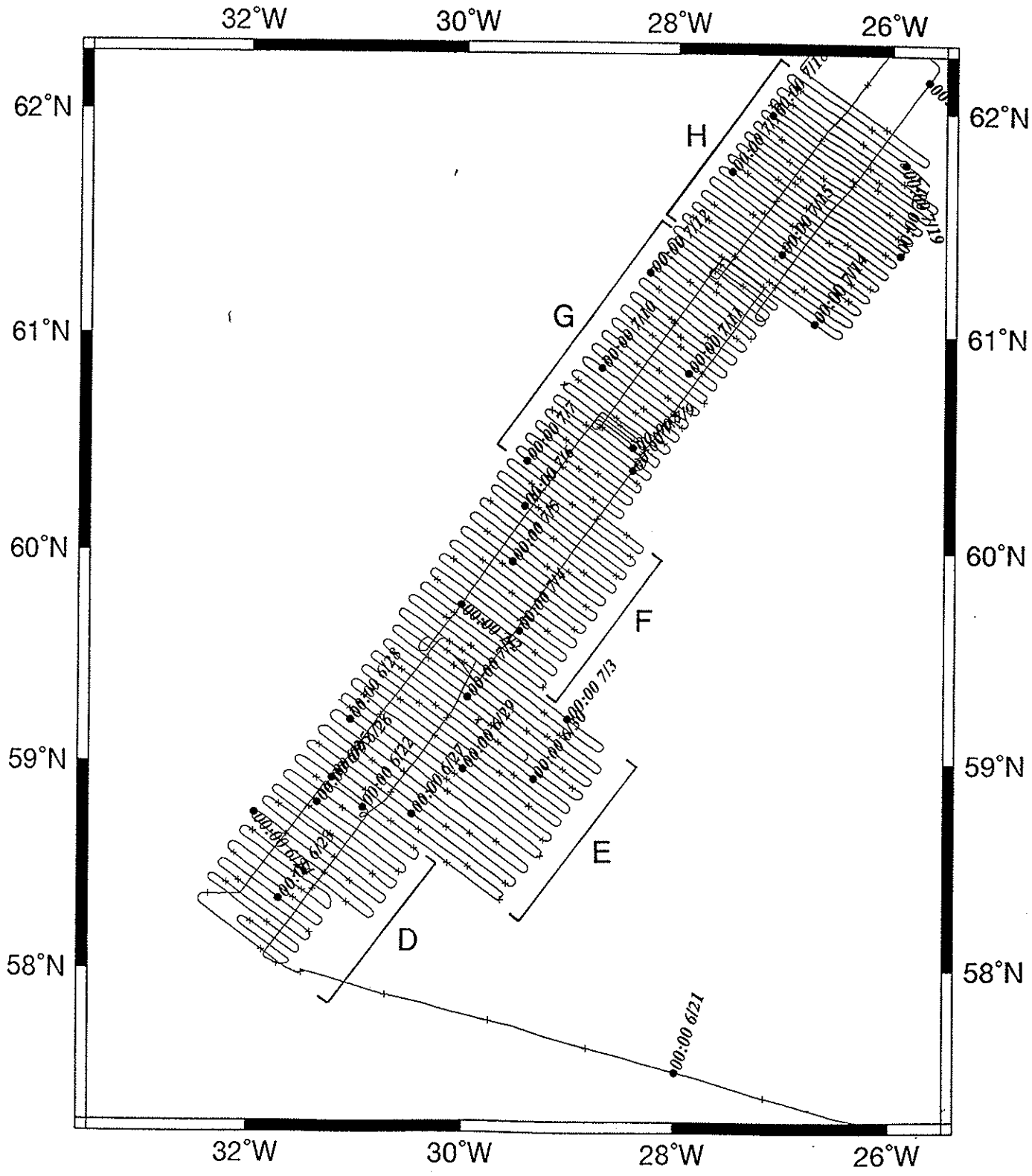

Figure 1 CD87 ship track. 0000Z is annotated every day, and the tickmarks are placed every 3 hours. The survey blocks are labelled D, E, F, G and H.

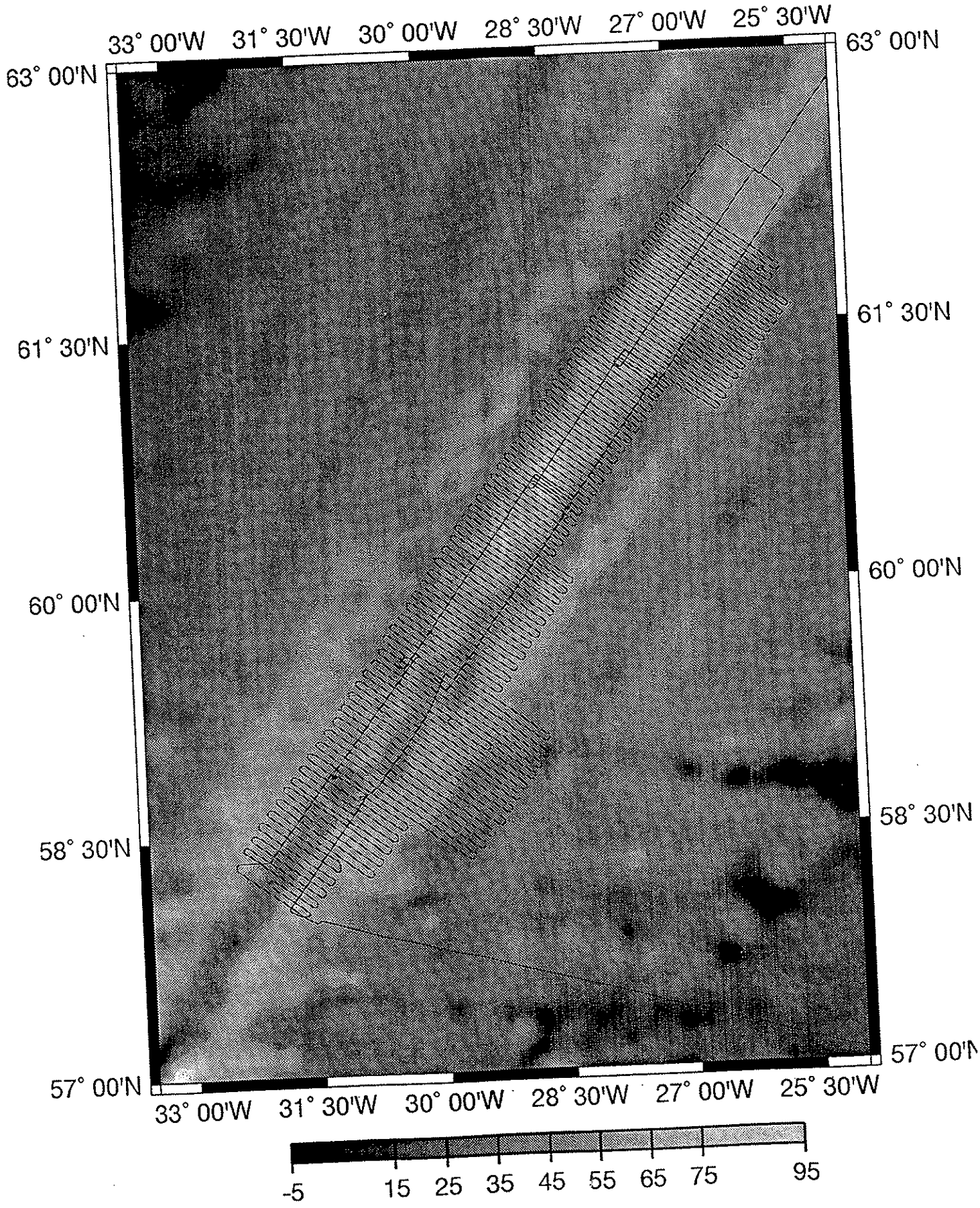

Figure 2 CD87 ship track superimposed over satellite gravity map. Scale bar is in mGal.

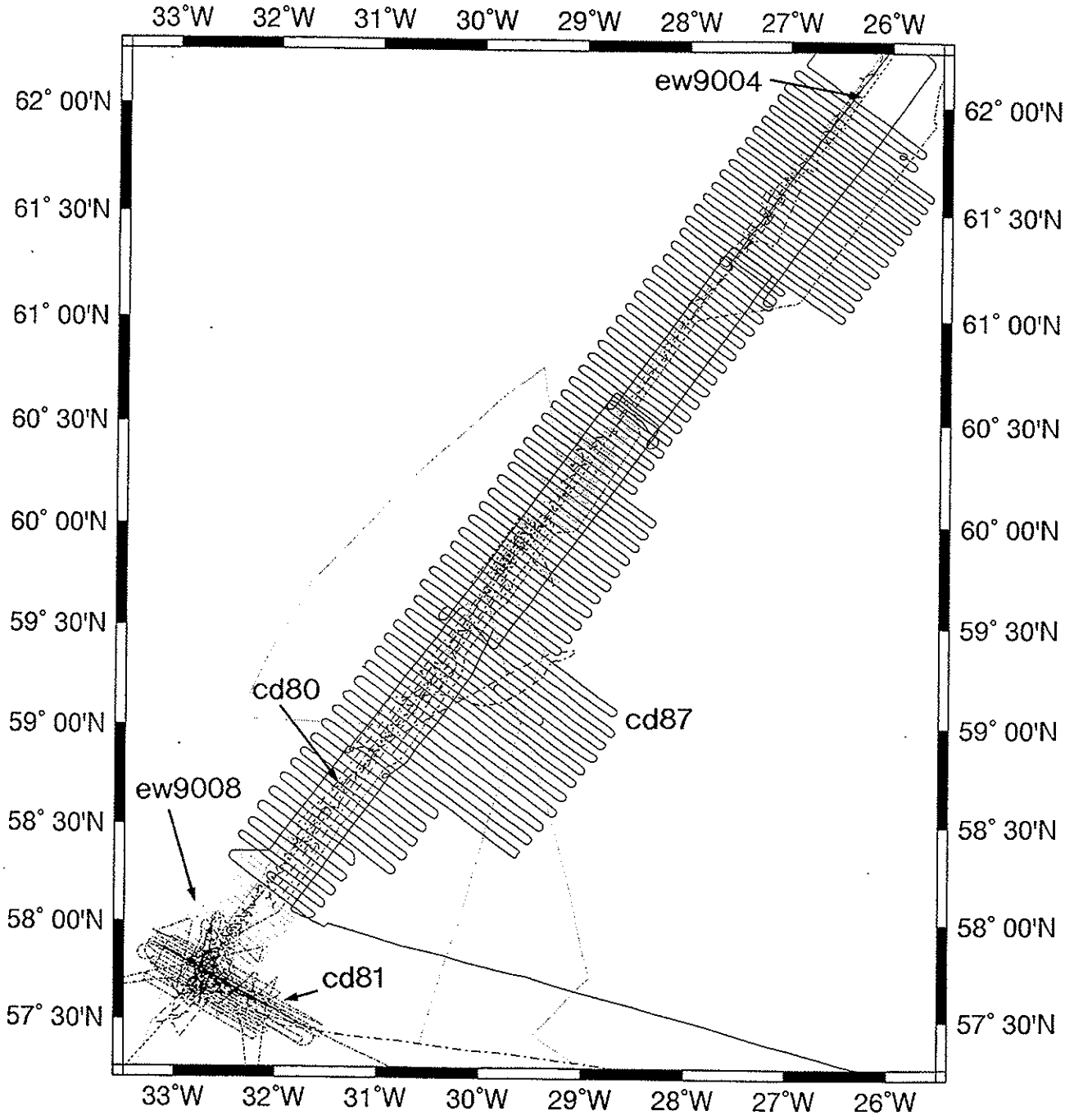

Figure 3 CD87, EW9004, EW9008, CD80 and CD81 ship tracks.

Tues June 21 (172)

1125: Slowing to recover magnetometer and carry out velocity dip.
1210: Start of velocity dip no. 2.
1322: Completed velocity dip. Relaunch magnetometer, resume course 285°.
1413: Start of Reykjanes Ridge survey, Area D, way-point 1 (see appendix A3 for waypoint listings). The survey begins at the northern limit of the 'EW9008 Area C', and the first few lines were designed to fill in between existing coverage from that cruise.
1851: Way point 4. A/c 036° for first of two tie-lines run parallel to ridge axis and outside existing multibeam coverage.

Wed June 22 (173)

1050: Ended tielines and filling in. Started first of 7 lines oriented ridge-perpendicular and spaced initially 4.5 km (way-point D12).
1437: Increased line spacing to 5 km. This still gives almost 100% coverage.

Thur June 23 (174)

1452: Way-point D26. Line length increased to 80 km to examine southern termination of 'V-shaped ridge', for the next 9 lines.

Fri June 24 (175)

Area D survey continued.

Sat June 25 (176)

0724: End of Area D survey (waypoint D45).
0758: Commenced tie-lines for Area E (waypoint E1)
Weather worsening towards evening.
2036: Tie-lines complete; commencing main Area E survey with 130 km-long-lines (way-point E6).

Sun June 26 (177)

Full Gale by morning. Ship slowed to 5 knots; EM12 missing pings frequently. Air in sound velocity tank preventing sensible readings.
1800: First plots of gridded bathymetry and magnetics produced for Area D. Weather abating.
2400: Back to full speed.

Mon June 27 (178)

Good weather. Survey E continuing.

Tues June 28 (179)

Good weather. Survey E continuing. Making speeds of almost 12 knots.
2009-2100: Fifty minutes of data lost from EM12 when active logging file accidentally deleted.

Wed June 29 (180)

Sea continuing very calm, with light swell.
0949: Line spacing reduced from 5.0 km to 4.5 km after waypoint E29.

Thur June 30 (181)

Weather still calm. Clear skies, and continuous twilight tonight. Slight fog in morning.
0831: EM12 stopped transmitting - communications error? Not immediately noticed by watchkeeper.
0938: EM12 restarted.
1451: Looped round to fill gap on previous line caused by morning's transmission loss.
1700: Back on course.

Fri July 1 (182)

2157: Way point E47. Turned north for tie-lines of area F.
2242: Way-point E48. Start of tie-lines.

Sat July 2 (183)

1352: Way-point F3. End of tie-lines.
1502: Way-point F4. Resuming last lines in area E.

Sun July 3 (184)

0443: End of Area E (way-point E53).
0506: Start of Area F, with lines shortened to 80 km (way-point F5).

Mon July 4 (185)

Tues July 5 (186)

Weather remains fair.
EM12 plots of areas C, D, and E have now been completed.

Wed July 6 (187)

Wind raised somewhat - force 6 by afternoon, but still making ca. 11 knots.

Thur July 7 (188)

Wind 30 knots, slowing us on some headings.
0015: Way-point F48. End of Area F.
0038: Start of area G, with lines shortened to 60 km. (way-point G1).

Fri July 8 (189)

Strong winds continue. Speed down to 4.5 knots at times.

Sat July 9 (190)

Sun July 10 (191)

Weather improving after three days of gales.

Mon July 11 (192)

Line-spacing kept at 4 km because of time lost in bad weather. This causes some (10-20%) swath underlap at axis, but much of this is filled by earlier cruises.

Tues July 12 (193)

Started tie-lines for Area H, at site of CD70 seismic experiment.

Wed July 13 (194)

Barometer fell sharply in small hours.
0133: Way-point H3. Commencing second tie-line, SW along ridge axis. Very slow progress into head seas.
1300: Speed dropped to 3.5 knots.
1328: Tie-lines complete.
1413: Resuming last lines of Area G.
1920: Way-point G78: end of survey area G.
1940: Way-point H5. Commence 93 km-long 125°/305° lines for 'Cambridge' survey in area of CD70 seismic experiments.

Thur July 14 (195)

Weather began to improve, but some courses still slow.
2300: Speed 6.2 knots.

Fri July 15 (196)

Weather gradually improved throughout day.

Sat July 16 (197)

Wind 20 knots (the lowest for days!) Back to speeds of 11.5 - 12 knots.

Sun July 17 (198)

Good weather. Survey H continues.

Mon July 18 (199)

1721: Polarisation failed on magnetometer.
1740: Magnetometer repaired and running again.
2240: EM12 stopped pinging during turn at 12 knots. Looped round while attempting to restart equipment.
2338: EM12 working again.

Tues July 19 (200)

00:24 Rejoined survey line; short distance at start of line lost.
1124: WP 60: end of main Area H survey. Turned NW to reach continuation of northern cross-axis leg of tie-line.
1327: A/c to SE, toward WP H3, in order to link with the northern arm of the Area H tie-line and thus complete one further cross-axis traverse.
1457: End of cross-axis line. Slowing to recover magnetometer.
1521: Magnetometer recovered. A/c to NE for Reykjavik.
1600-1700: One hour's EM12 data lost because Mermaid failed to recommence logging after change of 'line' (file) number.
1937: EM12 switched off at 63°N. Scientific watches ceased.

Wed July 20 (201)

0549: Commenced short gravity survey off-shore Reykjavik for University of Iceland Science Institute (L. Kristiansson).
0819: Completed gravity survey.
1000: Docked in Reykjavik.

5. EQUIPMENT REPORTS

5.1 EM12S-120

During the cruise, the Simrad EM12S-120 ran continuously for 720 hours. Overall, the system performed excellently, gathering data of a superb quality. 5 hours data were lost when the Mermaid logging system locked up (this was fortunately on the passage to the work area), 1 hour when Mermaid failed to respond after the main survey and a total of 4 hours lost with Bottom Detection Unit (BDU) lock ups. The BDU is responsible for determining the range to the seafloor of every beam. A full calibration was carried out at the beginning of the cruise. Four sound velocity profiles were taken and XBTs deployed most days (see appendices A4 and A5), weather permitting.

5.2 LaCoste and Romberg Gravitymeter S40

The gravitymeter sensor and platform electronics were installed in the electricians store close to the pitch/roll centre of the ship and the logging and control electronics in the constant temperature laboratory alongside the Bell gravitymeter. Apart from a gyro change on day 168 and a "full hard disk crash" on day 199, the meter operated reliably throughout the cruise.

5.3 Bell Gravitymeter BGM3 SN 203

A loaned unit from the National Research Laboratories, Washington D.C was initially installed in the Research Vessel Base at Barry and apart from some instrumental drift during temperature stabilisation, in port checks confirmed its serviceable operation. The meter was transferred to RRS *Charles Darwin* and installed in the constant temperature laboratory and, apart from an initial malfunction indication during platform erection due to an unseated card in the Platform control power supply, the meter appeared to be operating correctly. Once a suitable Gaussian filter had been written to smooth the raw count data coming from the Pulse Rate Converter (PRC), it became apparent that during periods of rough weather this output was exceeding the stated range of between 5 and 45 kHz, and when this occurred the filtered output became noisy with consequent spikes. The sensor sub assembly and PRC electronics were checked by introducing "TEST" and "CALIBRATE" signals into them and logging the output over a two hour period. This appeared to suggest that the sensor subsystem electronics were operating correctly and the fault was confined to the sensor itself or associated electronics. Communications from Bell Aerospace via NRL suggested that the time period of the Low Pass filter components within the Summing Amplifier was too small to prevent saturation of the Pulse rate converter under high acceleration conditions and such components, being within the sensor assembly, were not serviceable at sea.

5.4 Varian Magnetometer V75

Worked well throughout the cruise apart from a failure in the polarisation supply circuitry (Day 199). The unit was replaced with a spare which worked satisfactorily for the remainder of the cruise. Both systems have a good signal to noise ratio, however they still suffer from radio transmission interference at some frequencies.

5.5 Computer Systems

The RRS *Charles Darwin* is equipped with a third generation distributed data collection and processing system which is based on a three level architecture: level A samples and time-stamps data collected from the scientific instruments and navigation devices on board; level B logs and backs up the data; while level C performs the processing of the data. Minor hardware problems were fixed on board; however, most problems encountered were due to heavy loading of the network. Huge quantities of data were collected by the EM12S-120, which filled up disk space rapidly and was constantly being transferred across the network.

Regarding the multibeam processing, Neptune 2 processing, data logging (Mermaid) etc. were carried out on the shipboard computer system situated in the scientific plot on the Darwin. For MB-System processing, we brought a Sun Sparc 10 computer, with 2.5 Gbyte external disk drive, plus exabyte and optical drives, and networked it with the shipboard systems.

6. DATA PROCESSING

6.1 EM12S-120

6.1.1 Data handling All EM12S-120 data are logged using the Mermaid system in the form of datagrams - e.g. depth, position, sidescan etc. - all held in one 'raw' file. We chose to log amplitude and phase data as well as the crucial depth, position, sound velocity etc. The depth datagrams are actually recorded as depths rather than travel times, since the travel time to depth conversion, using sound velocity profile data, is performed prior to logging. We created new logging files hourly and they still reached some 12 Mb in size. All in all, throughout 30 days of EM12S-120 operation, we collected approximately 10 Gbytes of data. 80% of these comprised the amplitude and phase datagrams (if one were to log just pure amplitude datagrams, the volume would be reduced to a third). Raw data were transferred from the Mermaid logging workstation to an additional computer, then downloaded to both the Neptune and Durham machines for processing.

There were too much data for it all to reside on the hard disks of either the shipboard or Durham computers, so regularly throughout the cruise backups had to be made. These were done principally on exabyte (RVS) and optical disk (Durham - until we ran out of disks! - then exabyte). It is important to note that the ping rate of the EM12S-120 (and therefore data rate) varies according to water depth. Pulse lengths also vary between deep and shallow modes (Simrad, 1992); the threshold point is a water depth of approximately 1500 m - a typical depth over the Reykjanes Ridge. We generally collected data at a higher rate as we progressed through shallower water towards Iceland.

Intermediate processing products, such as edited hourly files, plus final grids and ancillary data also had to be backed up and archived. Processing typically requires intermediate storage 2 to 3 times the volume of the raw data.

6.1.2 Processing outline The basic stages for any multibeam processing procedure are to:

1. Merge bathymetry with navigation
2. Edit the bathymetry data
3. Grid
4. Display

6.1.3 MB-System bathymetry processing MB-System (written by Dave Caress and Dale Chayes of Lamonth Doherty Earth Observatory) is based on a modular concept, output can be either NetCDF or ASCII and it directly links with the widely used GMT package (Wessel & Smith, 1991). Refer to Caress & Chayes (1994), Owens (1994) and Blondel & Parson (1994) for further details.

An initial link is required between the Simrad raw datafiles and MB-System. Simrad provide a series of input/output libraries to deal with their data formats, however we

read them directly. First each raw datafile must be split into its constituent datagram types (*em12_divide_grams*), then the depth and position data must be merged into one file (*raw_gram_merge*). These position data are the raw navigation logged direct from a GPS receiver, though smoothed navigation (output from the shipboard ABC computer system) can be substituted at a later stage within MB-System (mbmerge). MB will now read in the EM12S-120 data (recognised by its own specific id - Hydrosweep, Sea Beam etc. have their own ids). These initial procedures can simply be incorporated into a shell.

The next stage in multibeam processing is to edit the data. MB-System includes both automatic statistical (mbclean) and manual interactive (mbedit) editing. The statistical methods include rejection of slopes greater than a critical value, removal of a specified number of outermost beams etc. However, from viewing our data ping-by-ping, the artifacts are not necessarily predictable and would not be easily distinguished statistically (or by eye sometimes!), particularly since we were surveying over rugged mid-ocean ridge terrain. We found that interactive editing was essential. Some typical artifacts were:

- occasional 'curl-up' of outermost beams
- 'loses bottom' on steep slopes (across- and along-track)
- spurious depths from outermost (and very occasionally other) beams
- whole ping recorded as 'parabola' (bad weather - attitude sensor problems)

Figure 4 presents some examples of these artifacts. We shall not attempt to explain the reasons for the artifacts here, though the reader could refer to de Moustier & Kleinrock (1986) for further details (they specifically deal with Sea Beam, but some of the problems are similar). We certainly recommend viewing the data in this manner to ensure artifacts are not interpreted as geological features and to realise the limitations of the system when imaging steep fault scarps, for example.

Generally the data were of very high quality. We were able to keep up editing with the data collection rate thanks to careful editing by watchkeepers (taking something like 6-8 man hours per day). On such a cruise though, other watchkeeping duties are limited.

After incorporation of smoothed navigation, the bathymetry data are ready to be gridded. The mbgrid routine limits the array sizes for gridding (somewhere around 300×300 nodes), so large areas must be divided into blocks, then pasted together after gridding (using GMT's grdpaste). Gridding is based on a Gaussian weighted scheme, which can be supplemented by interpolation (thin plate spline) over the data gaps.

Plots were generated using MB and the GMT freeware package (Wessel & Smith, 1991) and hardcopies made on any postscript printer. We managed to produce a large scale, colour-fill plot of all the data onboard (even though it involved sellotaping together almost 200 A4 sheets!). Figure 5 presents a scaled down version of the final grid.

a)

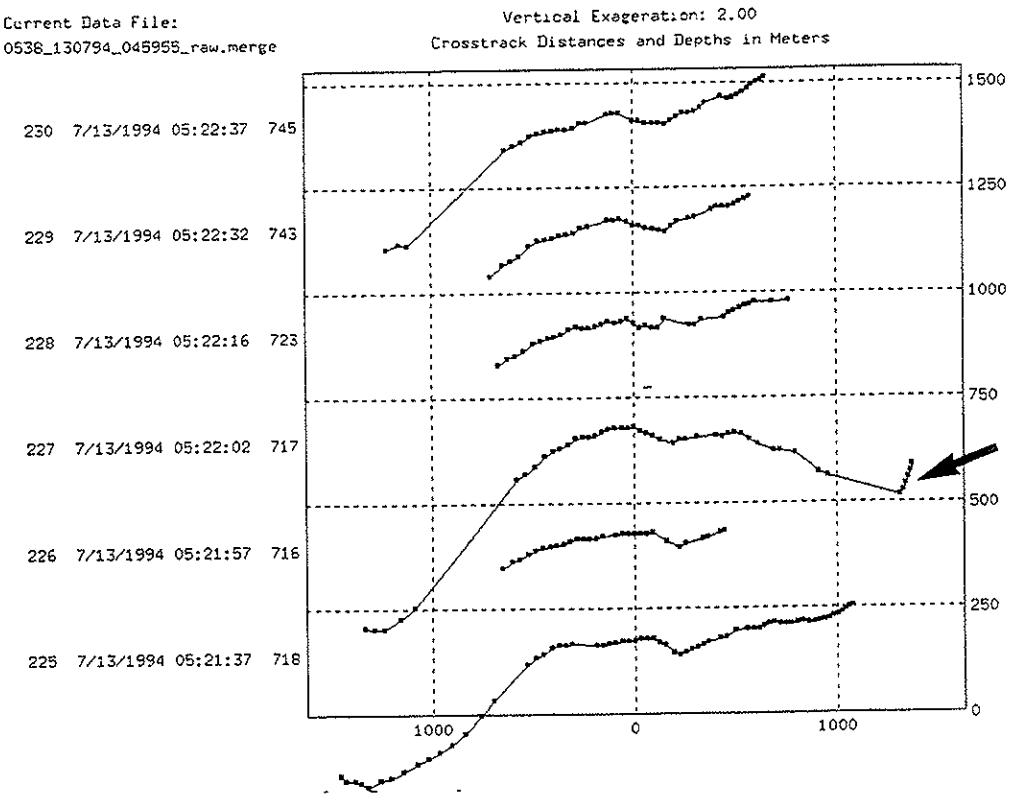

b)

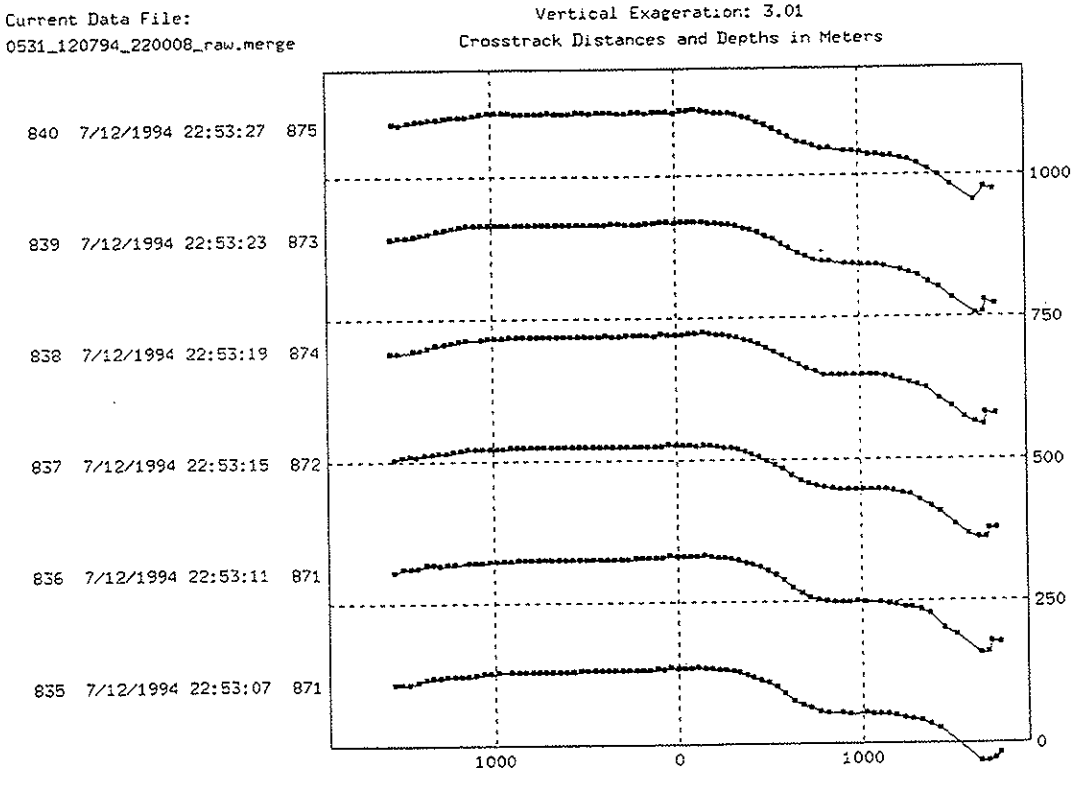

Figure 4 Examples of some typical EM12S-120 artifacts identified during editing: a) 'curl-up' of outermost beams; b) spurious depths from outermost beams.

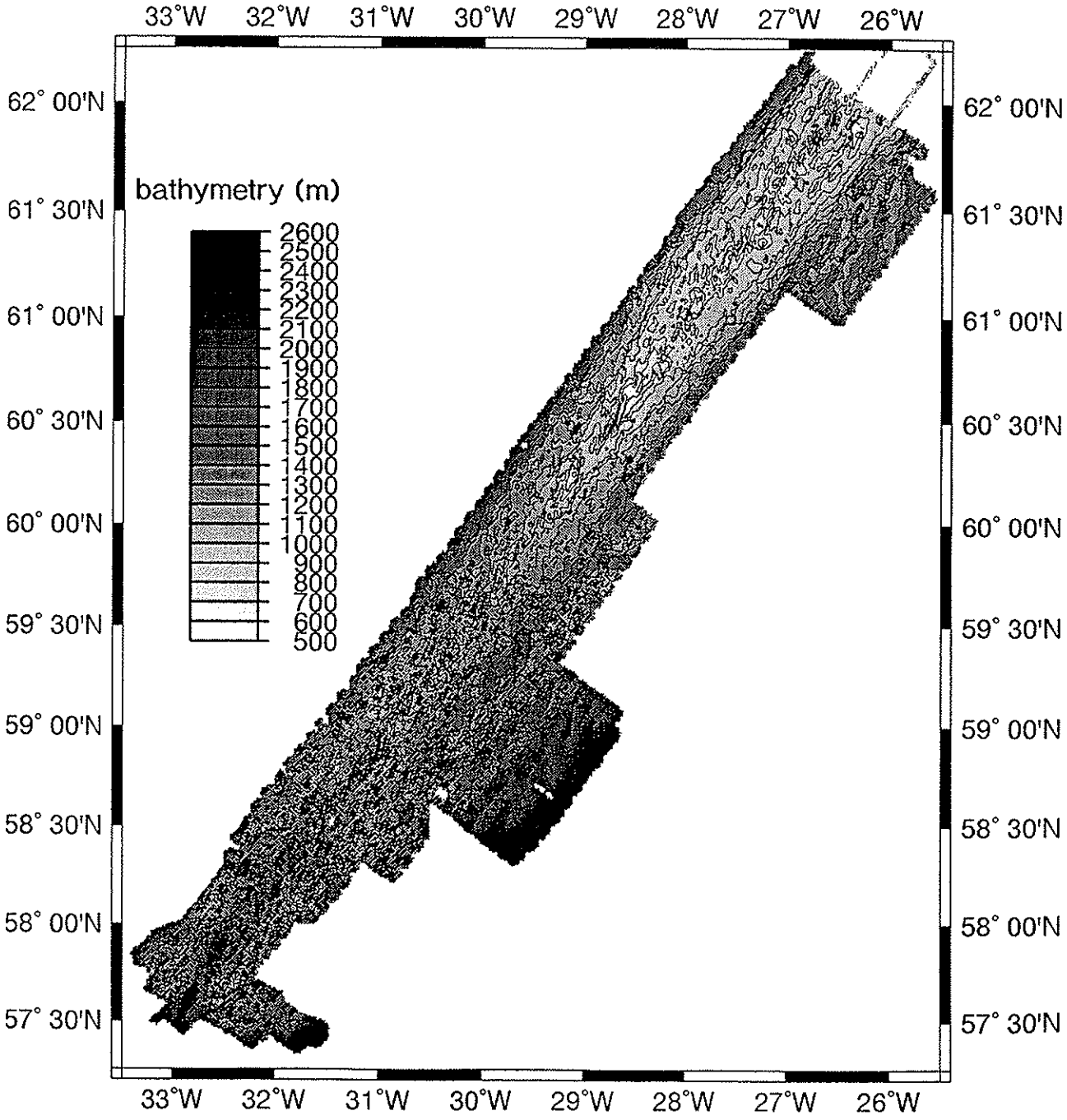

Figure 5 CD87 bathymetry data. Contour and grey scale at 100 m intervals.

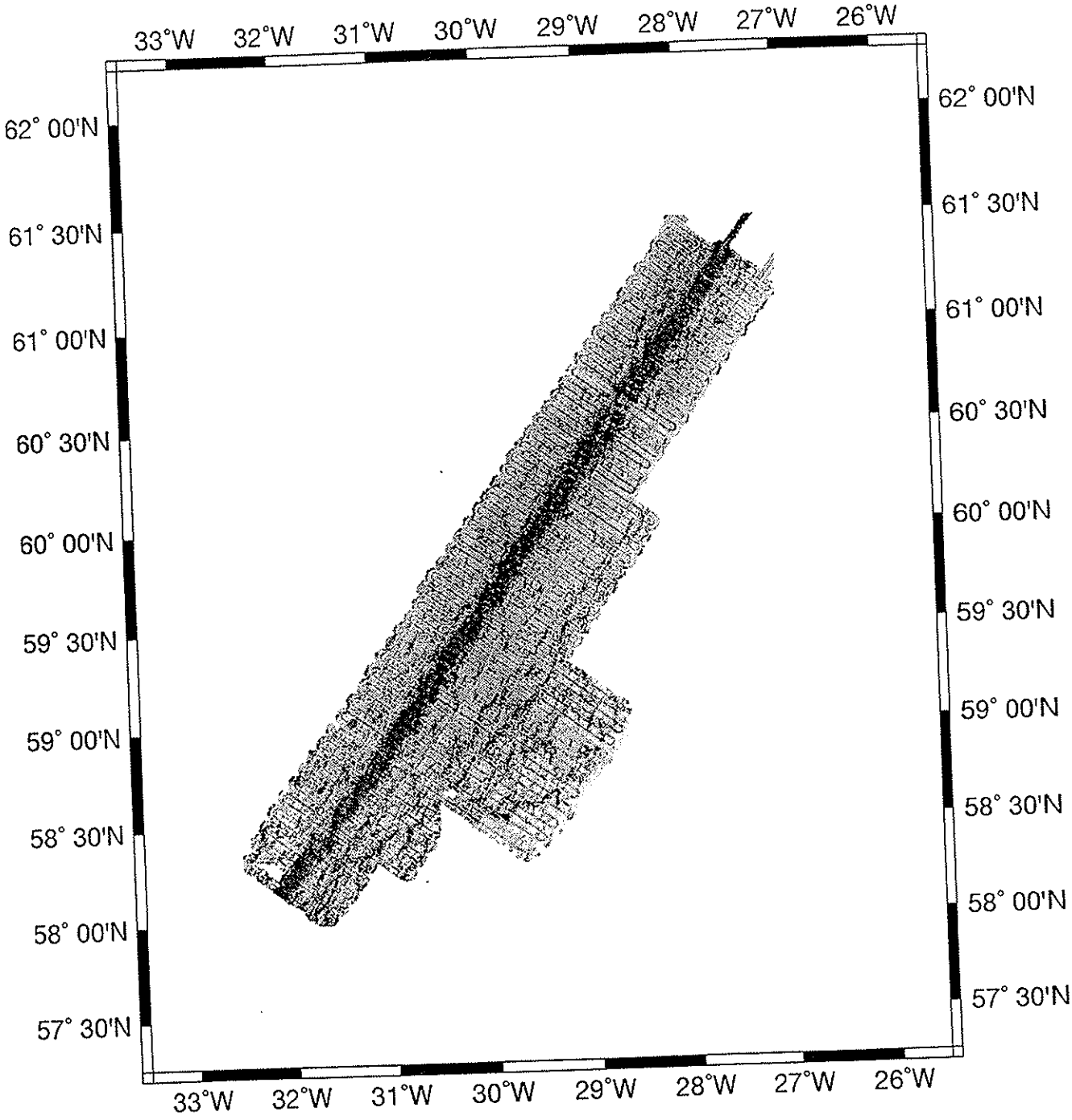

Figure 6 CD87 sonar imagery data. Black is equivalent to 0 dB, white to -64 dB.

6.1.4 Neptune 2 bathymetry processing Neptune 2 is the standard bathymetric, data processing and cleaning package provided by Simrad A/S for use with the EM series of multibeam echo sounders. The Neptune 2 system enables editing, correcting, cleaning, thinning, terrain modelling and plotting, given data transferred from the Mermaid logging system and other sources. The processing of data is performed in four dedicated modules, which are presented using X11/Motif:

- Position Processing - including spike removal, smoothing and merging positions from different sensors.
- Depth Processing - corrects for systematic errors, such as caused by an incorrect sound velocity profile (recalculation, editing), offset errors (e.g. time, roll, pitch, gyro, heave etc.) and also estimates depth errors.
- BinStat Data Cleaning - statistical calculations are performed on depth data, defined within geographical blocks. All depths from any line in a survey that fall into a block are read, gridded and analysed with the statistical information of the cells being presented as colour coded maps. A range of correlation plots (one depth aspect versus another) exist which help the user to spot problem areas, and the data cleaning tools of BinStat can be used to clean the data. The XYZ point data can be output in ASCII and binary form.
- Terrain Modelling and Plotting - an application of IRAP (Interactive Reservoir Analysis Package) written and supported by Geomatic A/S. Typical functions include the input/output of different file formats, fast and accurate gridding, terrain modelling, geodetic transformations, contouring, cross sections, 3D plots etc.

The Neptune 2 processing routine during CD87 was to establish a set of data blocks within pre-defined work areas, clean the data in each of the blocks using the BinStat module and then grid using IRAP. The Position Processing module was not required because the smoothed navigation was transferred from the shipboard ABC system and the Depth Processing Module was not used because the calibration offsets were set at the data source.

6.1.5 Sonar imagery processing The amplitude and phase datagrams were logged but not consulted any further onboard ship. However in the EM12S-120 depth datagrams, mean beam amplitudes are recorded alongside depths. Using MB-System, we were able to construct rudimentary 'sidescan' mosaics for all the cruise data, which proved very useful in defining zones of recent volcanism (figure 6 displays the amplitude data processed on board). Keeton and Mitchell (1994) describe the interpretation of multibeam sonar images. One must note the data volume and processing capacity that would be required to process the 'full resolution' imagery - the mean beam amplitudes are certainly sufficient for starters.

6.1.6 Summary Both Neptune 2 and MB-System provide excellent means for processing EM12S-120 multibeam bathymetry data. The packages are quite different in concept, design and interface style. Neptune 2 is permanently installed and supported on the Darwin, however MB is freely available to universities/institutes and

well-documented source code is available. Both systems operated successfully, and could produce the gridded product and maps by the end of the cruise. We only switched the EM12S-120 off 24 hours before arriving in port, and the last (sizeable) block of data was processed and printed out in time. Additionally, the volume of data collected and size of processing products emphasises the importance of careful backing up and quite what is involved (capacity-wise) in terms of archiving facilities.

6.2 Gravity

Crossover adjustment was performed on the LaCoste and Romberg data by an iterative matrix method and involved applying dc offsets to individual straight segments of data to minimise the overall rms crossover error. Before crossover adjustment, the rms crossover error was 6.8 mGal (figure 7a), which improved to 3.0 mGal after the adjustment (figure 7b).

It became apparent after examining cross-over errors and comparing profiles of the LaCoste and Romberg with the Bell BGM3 data, that the two gravitymeters were inconsistent between east to west and west to east survey lines. While on reciprocal courses, significant cross coupling errors (as large as 15 to 20 mGal) were evident, particularly during periods of moderately rough to rough weather. It was therefore decided to back off 6 days of gravitymeter data onto floppy disk from the gravitymeter hard disk during a sound velocity station, in order to do a cross correlation of cross coupling errors with gravity using a proprietary P.C. based program supplied by LaCoste and Romberg. The program calculates the optimum amounts of recorded cross coupling monitors to be added to gravity in order to eliminate any correlation between the curvatures (first derivative) of the monitors and gravity. The process was undertaken twice; once by utilising the recorded cross coupling and once by omitting it in order to verify the fractions contained within the cross coupling parameter menu in the gravitymeter. Once corrected fractions had been calculated, these were used to recompute the recorded data and to compare the recomputed profiles against the Bell gravitymeter. A significant improvement of the data was noticed reducing the differences between the two profiles from 10 to 2 or 3 milligals in the worst cases observed, although some residual course dependent error still remained.

After the cruise, the entire dataset was re-processed to remove the cross coupling effects. Before crossover adjustment, the crossover errors now improved to 3.6 mGal (figure 7c), and after adjustment, these were reduced to a satisfactory 0.8 mGal (figure 7d). Tie-ins were made to gravity base-stations in Barry and Reykjavik, yielding a drift of 0.09 mGal per day. The free air gravity data are displayed in figure 8. A preliminary mantle Bouguer anomaly was also produced on board.

6.3 Magnetics

Magnetic anomaly data were reduced to IGRF, but diurnal and storm variations were not removed (figure 9). The anomalies were inverted to crustal magnetisations on board, using the method of Parker and Huestis (1974).

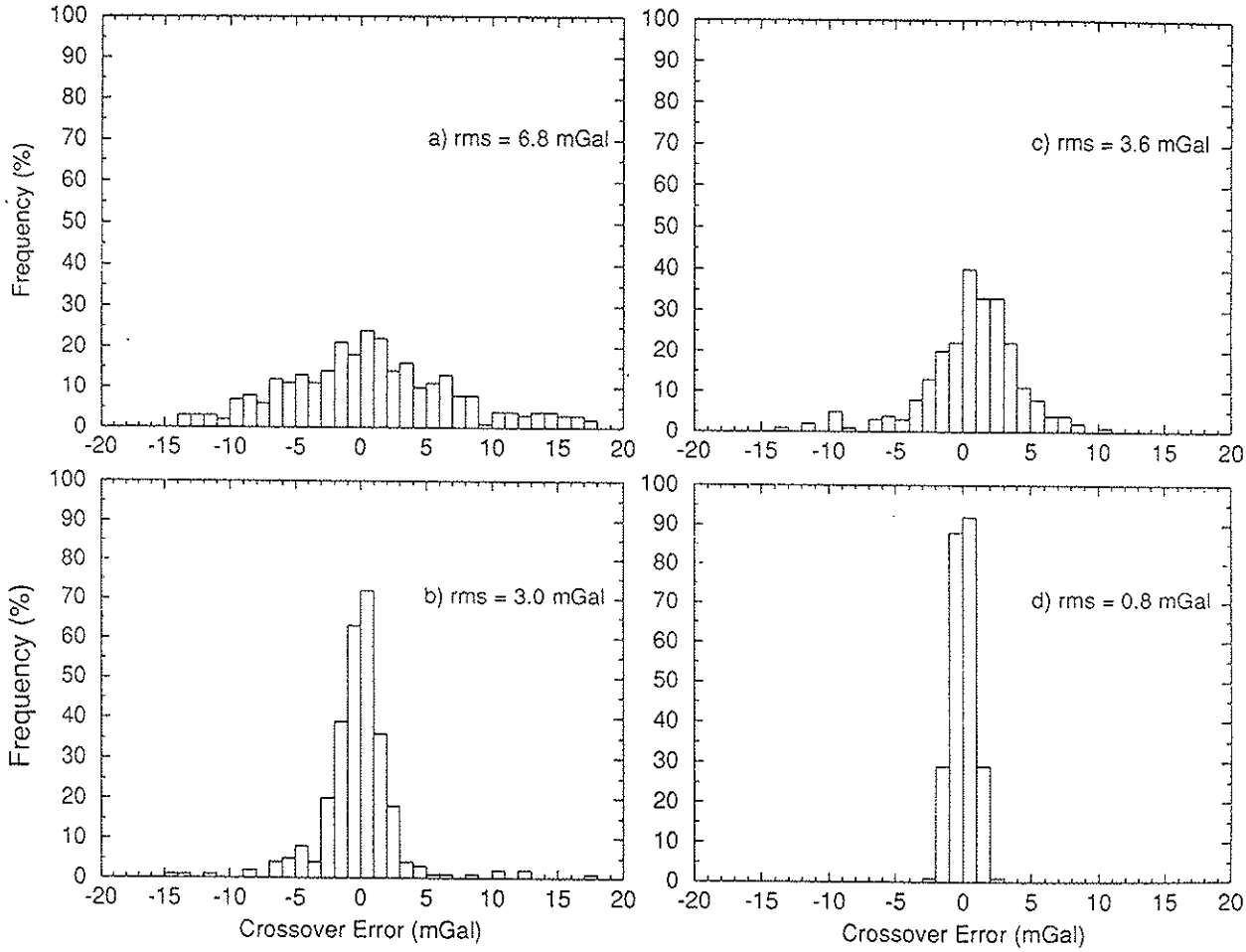

Figure 7 Crossover adjustment statistics for CD87: a) crossover errors before adjustment; b) crossover errors after adjustment; c) crossover errors before adjustment and after cross coupling correction; and d) crossover errors after adjustment and cross coupling correction.

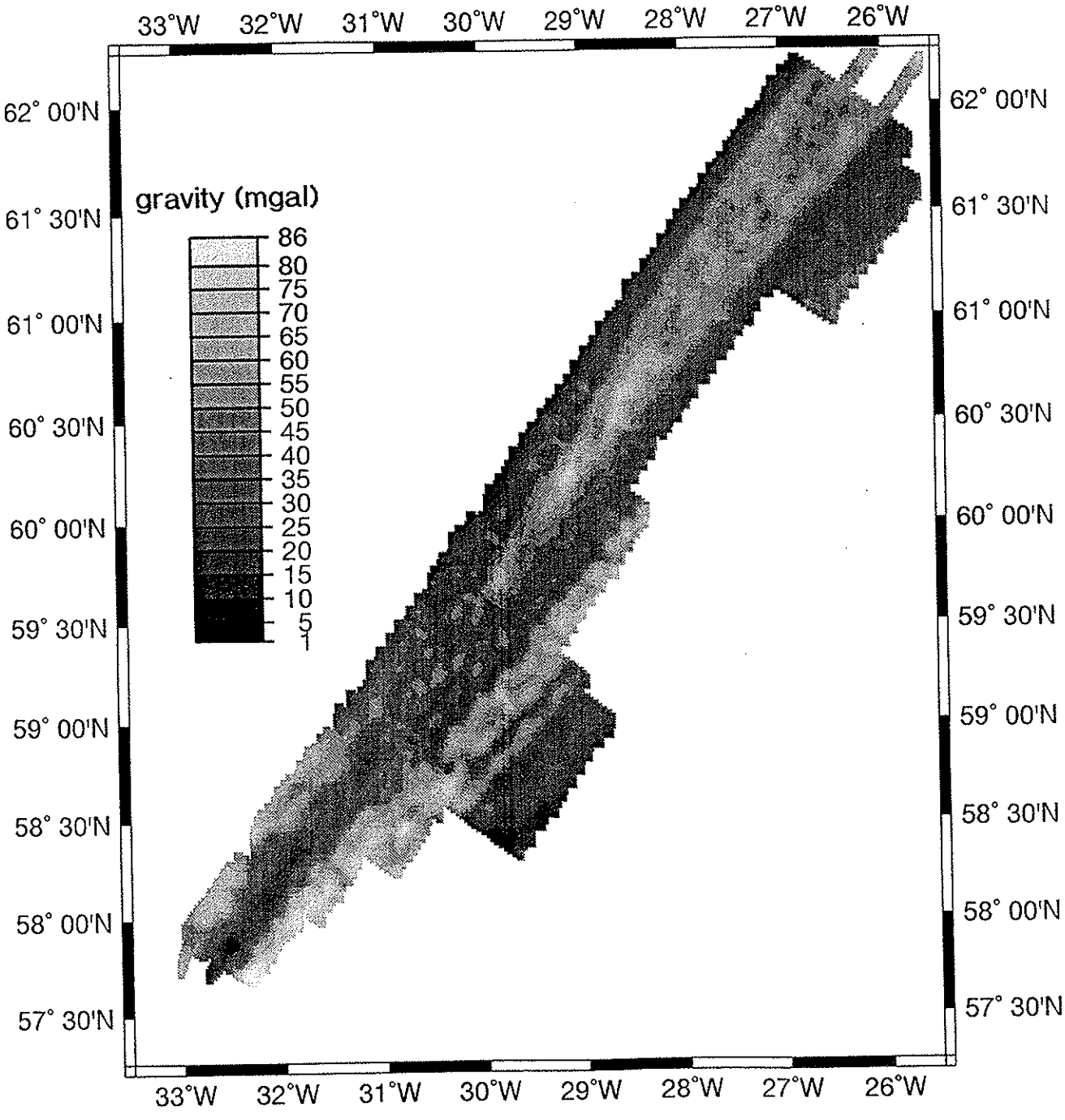

Figure 8 CD87 free air gravity.

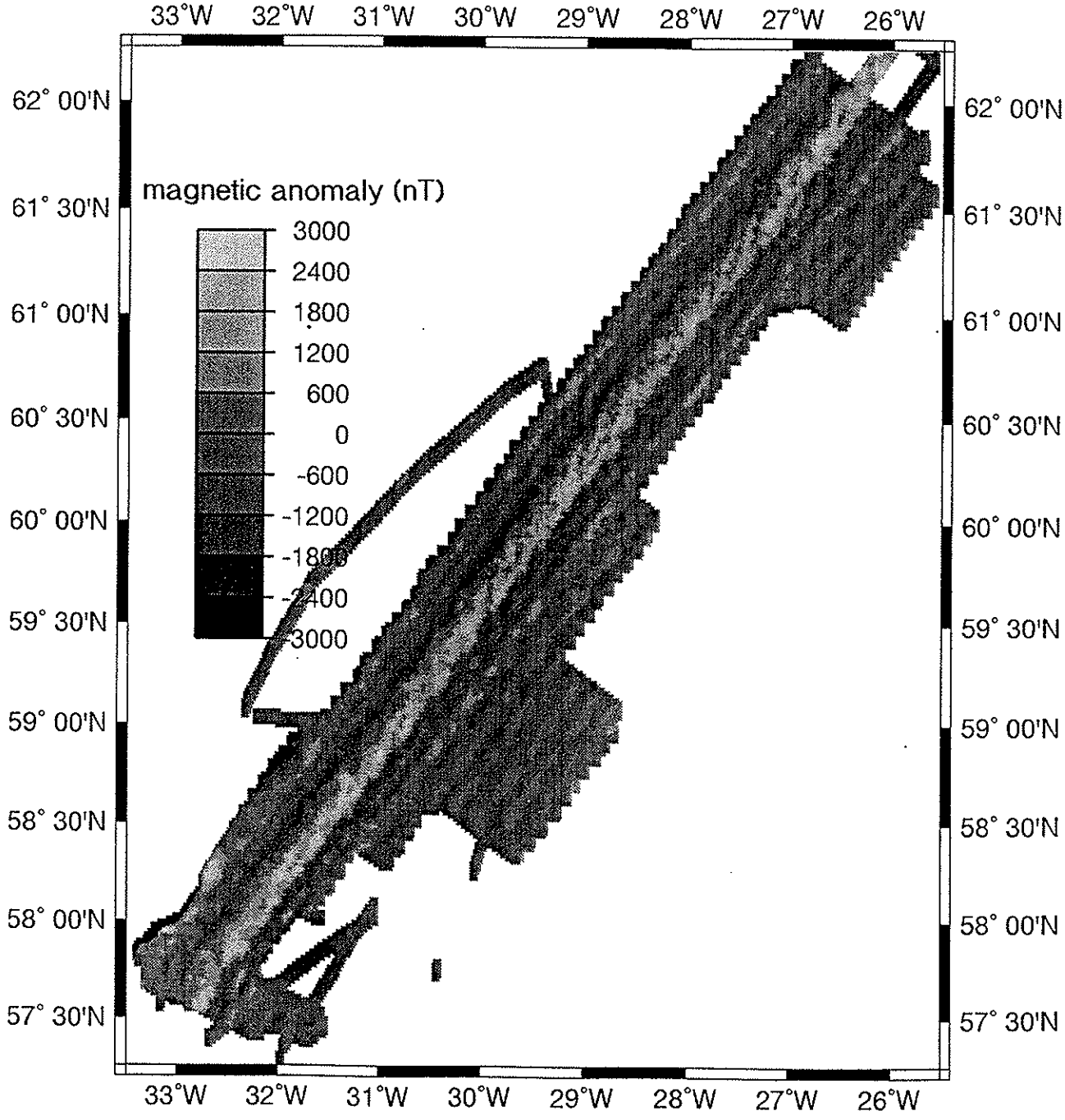

Figure 9 CD87 magnetic anomaly data.

7. PRELIMINARY CONCLUSIONS

Based on our initial shipboard examination of the data, some very preliminary conclusions are as follows:

We find that the Reykjanes Ridge axis and flanking isochrons are extremely linear and suffer no significant offsets for at least 580 km north of 57°55'N. Over the whole of this distance the ridge axis is 36° oblique to the spreading direction. There is an ubiquitous pattern of en echelon axial volcanic ridges (AVRs) sub-normal to the spreading direction along the whole length of Ridge surveyed.

Relict Axial Volcanic Ridges are most frequently seen off-axis where there is least axial faulting, tending to confirm that elsewhere they are rapidly eroded by faulting, as suggested previously by Parson et al. (1993). The axis is flanked by normal faults that are sub-parallel to the Ridge axis, the innermost of which occur slightly closer to the axis as one goes towards Iceland. Although the amplitudes of AVRs and faults varies along and across the ridge, the basic plan view pattern does not. We believe this pattern represents the basic response of the lithosphere to oblique spreading.

Generally, the amplitude of faulting decreases as Iceland is approached. In particular, there is negligible large-scale faulting near the axis north of the 'median valley/axial high' transition, which occurs near 58°50'N. However, towards the northern end of the Ridge (61°15' to 61°55'N) some near-axis small-scale faulting returns. Thus the morphology does not change in a simple monotonic manner as the Iceland hotspot is approached. The central part of the area studied (about 59° 40'N to 61° 15'N) appears to represent one end member, with large numbers of central volcanoes, no large-amplitude near-axis faulting, and no median valley. It also has the most linear and symmetric magnetic isochrons. To the north and south, the amplitude of faulting increases, the density of volcanoes decreases, and isochrons show a greater tendency for asymmetric spreading, nonlinearity or small offsets. Most of these variations probably reflect changes in mantle temperature, and the culmination of them in the central region suggests the existence there of a local temperature high, possibly reflecting a transient pulse of high plume output and perhaps the latest (previously unrecognised) V-shaped ridge.

There is an axial zone of high backscatter, some 10-15 km wide, marking the zone of recent volcanic activity. The width of this zone remains approximately constant (apart from small local disturbances) along the length of the Ridge, and in particular does not depend on the existence of a median valley to delimit it.

Even where there is no sign of a median valley near the axis, flanking lines of high fault-blocks persist off-axis along the ridge length. Their heights vary along the ridge (suggesting a segmentation pattern) but they are not laterally offset. Relative highs and lows in these 'crestal mountains' tend to alternate from side to side across the axis, but, at least in the south, are slightly higher on the SE side.

The mantle Bouguer anomaly is very smooth, exhibiting little mid- to short-wavelength variation above a few mGal. Along-axis variations in the mantle Bouguer anomaly are of very low amplitude compared with other parts of the Mid-Atlantic Ridge.

The main 'V-shaped ridge' (which converges on the axis near 58°30'N) is morphologically discontinuous, being composed of lines of closely-spaced but distinct tectonic blocks. The innermost of these ridges comprises three closely-spaced, parallel bands of such elevated blocks. The ridge displays an internal tectonic fabric which is similar to that on the surrounding seafloor, but of higher amplitude (i.e. bigger fault scarps). There is no evidence of off-axis volcanic activity or abnormal numbers of volcanic seamounts on the V-shaped ridge. The gravity signal over the V-shaped ridge is of much greater amplitude than expected from the observed bathymetry, which suggests compensation via regional rather than pointwise local isostacy.

Magnetic anomalies are very linear, departing from great circles parallel to the axis by less than 15 km, mostly in a slow regional variation. Local kinks in the Brunhes of up to 3 km in along-axis distances of 20-30 km occur at 59°12'N, 60°23'N and 61°28'N; none of them are associated with significant morphological discontinuities. Similar kinks in older stripes are not aligned. A larger bend to near NS anomalies at 57°50'N affects most isochrons and is associated with offsets and missing anomalies, confirming this as the first significant ridge-axis discontinuity south of Iceland and suggesting a history of ridge jumping or propagation here.

Spreading has mostly been constant at 10.6 $\pm$ 0.3 km/My over the past 10 My, and has been symmetric to within 5% or better over at least the past 2.8 My. Exceptions are south of 57°50'N (see above), and north of 61°28'N where spreading appears to have been faster to the east since 2.8 My.

Magnetisation amplitude varies along all isochrons by factors of about 2 over distances of 15 to 35 km, much greater than the AVR spacing. These variations are weakly correlated with morphology: some highs occur near the southern ends of AVRs suggesting a possible link with AVR-scale magma propagation; some lows occur near the centres of AVRs suggesting possible influence from hydrothermalism or shallow isotherms. The variations are not aligned or correlated with the 'V-shaped' diachronous ridges or with distance from Iceland. A superimposed short- wavelength pattern correlates strongly with the en-echelon AVRs. We are testing whether it is real or a residual terrain effect incompletely corrected by the inversion. If real, it may reflect variations in mineral composition and/or crustal temperature at the AVR scale.

ACKNOWLEDGEMENTS

We wish to thank the master, officers and crew of the RRS *Charles Darwin* and the RVS technicians for all their help in ensuring a highly successful cruise. We also thank the Natural Environment Research Council (BRIDGE programme) for funding the work. Dave Caress and Dale Chayes of Lamont Doherty Earth Observatory are

acknowledged for the provision of the MB-System multibeam processing software. Bruce Appelgate, Sandy Shor (University of Hawaii), Christine Peirce (University of Durham), Martin Sinha (University of Cambridge), Lindsay Parson and Bramley Murton (IOSDL) are all thanked for providing data from their cruises.

APPENDICES

A1. Scientific Personnel

Professor Roger Searle	University of Durham	Principal Scientist
Dr Barry Parsons	University of Oxford	Co-Principal Investigator
Dr Jane Keeton	University of Durham	PDRA
Mr Robin Owens	University of Oxford	Ph.D. student
Mr Robin Mecklenburgh	University of Oxford	Ph.D. student
Ms Catriona Hepburn	University of Cambridge	Ph.D. student
Ms Cynthia Robinson	University of Cambridge	Ph.D. student
Mr Dave Booth	RVS	Instrument support
Mr Adrian Fern	RVS	Computer support
Mr Gareth Knight	RVS	Computer support
Mr Chris Paulson	RVS	Instrument support

A2. Ship's Personnel

J D Noden	Master
P W Newton	Chief Officer
T J Boult	2nd Officer
J C Holmes	3rd Officer
J G L Baker	Radio Officer
S A Moss	Chief Engineer
S F Dean	2nd Engineer
C J Phillips	3rd Engineer
S J Bell	3rd Engineer
G A Pook	CPO(D)
T G Lewis	PO(D)
P H C Dean	Seaman
H R Hebson	Seaman
J R Perkins	Seaman
R W G Avery	Seaman
C J Elliot	Catering Manager
G A Welch	Chef
P W Robinson	Steward
R F Murphy	Steward
F Hardacre	Steward
K Pringle	Motorman

A3. List of Way Points

Waypoint	Julian Day	Time	Latitude	Longitude
Area D				
D1	172	14:13	58.0133	328.3417
D2	172	17:32	58.2500	327.5517
D3	172	17:51	58.3617	327.6117
D4	172	18:51	58.3617	327.9333
D5	172	22:00	58.9100	328.7283
D6	173	00:08	58.7583	329.1333
D7	173	05:29	58.0817	328.1667
D8	173	06:27	58.0450	328.3867
D9	173	08:25	58.2183	327.9317
D10	173	08:53	58.2517	327.9767
D11	173	10:27	58.0783	328.4333
D12	173	10:30	58.1117	328.4783
D13	173	14:18	58.4283	327.6483
D14	173	14:37	58.4633	327.6917
D15	173	17:37	58.1450	328.5267
D16	173	18:00	58.1783	328.5767
D17	173	22:00	58.4950	327.7400
D18	173	22:18	58.5317	327.7917
D19	174	01:14	58.2150	328.6317
D20	174	01:37	58.2500	328.6850
D21	174	06:08	58.5667	327.8483
D22	174	06:41	58.6067	327.9067
D23	174	09:53	58.2950	328.7333
D24	174	10:20	58.3300	328.7833
D25	174	14:25	58.6467	327.9550
D26	174	14:52	58.6827	328.0070
D27	174	18:39	58.2540	329.1130
D28	174	19:03	58.2900	329.1650
D29	174	23:43	58.7190	328.0590
D30	175	00:10	58.7550	328.1110
D31	175	03:55	58.3260	329.2160
D32	175	04:20	58.3620	329.2680
D33	175	08:21	58.7910	328.1570
D34	175	08:28	58.8270	328.2090
D35	175	12:32	58.3980	329.3200
D36	175	12:56	58.4333	329.3667
D37	175	16:44	58.8460	328.2533
D38	175	17:08	58.8820	328.3057
D39	175	21:02	58.4693	329.4185
D40	175	21:22	58.5052	329.4702
D41	176	00:57	58.9178	328.3582
D42	176	01:20	58.9538	328.4107
D43	176	05:26	58.5412	329.5222
D44	176	05:54	58.5772	329.5740
Area E				
D44	176	05:54	58.5772	329.5740
E1	176	07:58	58.7467	329.1167
E2	176	08:43	58.8167	329.2833
E3	176	12:16	59.2500	329.9000
E4	176	14:30	59.4833	330.1167
E5	176	15:29	59.6000	329.8000
E6	176	20:12	58.8900	328.7283
E7	176	21:38	58.9900	328.4633
E8	176	22:15	59.0267	328.5150
E9	177	08:45	58.3417	330.3317
E10	177	09:34	58.3783	330.3833
E11	177	20:24	59.0617	328.5850
E12	177	20:51	59.0967	328.6183
E13	178	03:05	58.4150	330.4383
E14	178	03:34	58.4483	330.4850
E15	178	10:09	59.1333	328.6717
E16	178	10:31	59.1700	328.7217

E17	178	16:33	58.4850	330.5367
E18	178	17:00	58.5217	330.5867
E19	178	23:15	59.2033	328.7750
E20	178	:01	59.2433	328.8333
E21	179	05:45	58.5577	330.6607
E22	179	06:10	58.5910	330.7093
E23	179	12:13	59.2817	328.8800
E24	179	14:40	59.3167	328.9300
E25	179	20:59	58.6310	330.7613
E26	179	21:24	58.6660	330.8148
E27	180	03:18	59.3517	328.9817
E28	180	03:43	59.3833	329.0333
E29	180	09:49	58.7017	330.8650
E30	180	10:10	58.7343	330.9120
E31	180	16:07	59.4200	329.0808
E32	180	16:31	59.4517	329.1267
E33	180	22:34	58.7667	330.9567
E34	180	22:58	58.7983	331.0033
E35	181	04:35	59.4850	329.1733
E36	181	05:19	59.5167	329.2200
E37	181	11:24	58.8317	331.0483
E38	181	11:48	58.8633	331.0933
E39	181	21:16	59.5500	329.2667
E40	181	21:33	59.5817	329.3117
E41	182	03:37	58.8967	331.1383
E42	182	04:00	58.9283	331.1850
E43	182	10:00	59.6150	329.3583
E44	182	10:20	59.6467	329.4050
E45	182	16:25	58.9617	331.2300
E46	182	16:48	58.9933	331.2750
E47	182	21:57	59.5850	329.7000
E48	182	22:41	59.5450	329.6700
F1	183	05:23	60.6500	331.2833
F2	183	06:44	60.4833	331.7333
F3	183	13:53	59.3983	330.1583
F4	183	15:00	59.5350	329.8333
E49	183	16:19	59.6883	329.4250
E50	183	19:42	59.7207	329.4717
E51	183	22:36	59.0595	331.2592
E52	183	22:58	59.0917	331.3050
E53	184	04:43	59.7533	329.5183
Area F				
F1	183	05:23	60.6500	331.2833
F2	183	06:44	60.4833	331.7333
F3	183	13:53	59.3983	330.1583
F4	183	15:00	59.5350	329.8333
F5	184	05:06	59.7850	329.5650
F6	184	08:52	59.3617	330.7150
F7	184	09:13	59.3950	330.7617
F8	184	12:57	59.8183	329.6100
F9	184	13:16	59.8500	329.6567
F10	184	17:00	59.4267	330.8083
F11	184	17:23	59.4600	330.8550
F12	184	21:08	59.8833	329.7033
F13	184	21:28	59.9150	329.7500
F14	185	01:15	59.4917	330.9017
F15	185	01:38	59.5233	330.9483
F16	185	05:25	59.9467	329.7967
F17	185	05:49	59.9800	329.8450
F18	185	09:40	59.5567	330.9950
F19	185	10:06	59.5883	331.0400
F20	185	13:50	60.0117	329.8917
F21	185	14:13	60.0450	329.9383
F22	185	18:07	59.6217	331.0867
F23	185	18:30	59.6533	331.1333
F24	185	22:12	60.0767	329.9850
F25	185	22:33	60.1083	330.0333

F26	186	02:22	59.6867	331.1800
F27	186	02:46	59.7183	331.2267
F28	186	06:25	60.1417	330.0800
F29	186	06:47	60.1733	330.1267
F30	186	10:38	59.7500	331.2733
F31	186	10:59	59.7833	331.3200
F32	186	14:31	60.2067	330.1750
F33	186	14:56	60.2383	330.2217
F34	186	18:46	59.8150	331.3667
F35	186	19:08	59.8483	331.4133
F36	186	22:48	60.2717	330.2683
F37	186	23:10	60.3033	330.3167
F38	187	03:05	59.8800	331.4600
F39	187	03:29	59.9117	331.5067
F40	187	07:08	60.3350	330.3633
F41	187	07:30	60.3683	330.4117
F42	187	11:32	59.9450	331.5550
F43	187	11:54	59.9767	331.6017
F44	187	15:38	60.4000	330.4583
F45	187	16:00	60.4333	330.5067
F46	187	20:12	60.0100	331.6483
F47	187	20:32	60.0283	331.6750
F48	188	00:15	60.4517	330.5083
Area G				
G1	188	00:38	60.4817	330.5517
G2	188	03:49	60.1638	331.4350
G3	188	04:16	60.1933	331.4783
G4	188	07:01	60.5117	330.5967
G5	188	07:24	60.5400	330.6400
G6	188	10:38	60.2233	331.5217
G7	188	11:00	60.2533	331.5650
G8	188	13:47	60.5700	330.6833
G9	188	14:10	60.6000	330.7283
G10	188	17:34	60.2833	331.6083
G11	188	17:56	60.3117	331.6517
G12	188	20:38	60.6300	330.7717
G13	188	21:00	60.6600	330.8150
G14	189	00:26	60.3417	331.6950
G15	189	00:52	60.3717	331.7383
G16	189	03:52	60.6883	330.8600
G17	189	04:15	60.7183	330.9033
G18	189	07:41	60.4017	331.7833
G19	189	08:22	60.4317	331.8267
G20	189	14:55	60.7483	330.9483
G21	189	16:03	61.3583	332.4283
G22	189	21:01	60.5750	331.2667
G23	189	21:38	60.6117	331.2667
G24	189	23:36	60.5083	331.5500
G25	190	00:12	60.4650	331.6117
G26	190	01:26	60.4017	331.7833
G27	190	02:02	60.4317	331.8267
G28	190	05:44	60.7483	330.9483
G29	190	06:20	60.7783	330.9917
G30	190	11:22	60.4617	331.8700
G31	190	11:53	60.4917	331.9133
G32	190	15:07	60.8083	331.0367
G33	190	15:42	60.8367	331.0800
G34	190	19:26	60.5200	331.9583
G35	190	19:51	60.5500	332.0017
G36	190	23:02	60.8667	331.1250
G37	190	23:29	60.8967	331.1700
G38	191	02:59	60.5800	332.0450
G39	191	03:25	60.6100	332.0900
G40	191	06:19	60.9267	331.2133
G41	191	06:40	60.9567	331.2583
G42	191	09:44	60.6400	332.1333
G43	191	10:12	60.6683	332.1767

G44	191	13:04	60.9850	331.3017
G45	191	13:27	61.0150	331.3467
G46	191	16:15	60.6983	332.2217
G47	191	18:33	60.7283	332.2650
G48	191	21:26	61.0450	331.3917
G49	191	21:46	61.0750	331.4367
G50	192	00:38	60.7583	332.3100
G51	192	01:00	60.7883	332.3533
G52	192	04:01	61.1050	331.4800
G53	192	04:21	61.1333	331.5250
G54	192	07:11	60.8167	332.3983
G55	192	07:33	60.8467	332.4417
G56	192	10:36	61.1633	331.5700
G57	192	10:57	61.1933	331.6150
G58	192	13:42	60.8767	332.4867
G59	192	14:07	60.9067	332.5300
G60	192	17:14	61.2233	331.6583
G61	192	17:36	61.2533	331.7033
G62	192	20:22	60.9367	332.5750
G63	192	20:45	60.9650	332.6200
G64	192	23:58	61.2817	331.7483
G65	193	00:17	61.3117	331.7933
G66	193	02:55	60.9950	332.6633
G67	193	03:24	61.0250	332.7083
G68	193	07:06	61.3417	331.8383
G69	193	07:28	61.3717	331.8833
G70	193	10:00	61.0550	332.7533
G71	193	10:17	61.0850	332.7967
G72	193	13:26	61.4017	331.9283
G73	193	13:48	61.4300	331.9733
G74	193	16:35	61.1133	332.8417
H1	193	17:14	61.1083	332.7500
H2	194	00:26	62.2083	334.4417
H3	194	01:27	62.3317	334.0800
H4	194	13:28	61.2650	332.3883
G75	194	14:11	61.3017	332.3867
G76	194	15:54	61.1350	332.8717
G77	194	16:21	61.1567	332.8867
G78	194	19:20	61.4600	331.9867
Area H				
H1	193	17:14	61.1083	332.7500
H2	194	00:26	62.2083	334.4417
H3	194	01:27	62.3317	334.0800
H4	194	13:28	61.2650	332.3883
H5	194	19:40	61.4883	332.0283
H6	195	00:35	60.9983	333.4767
H7	195	00:57	61.0250	333.5167
H8	195	05:33	61.5150	332.0683
H9	195	05:53	61.5433	332.1083
H10	195	10:20	61.0533	333.5550
H11	195	10:42	61.0800	333.5950
H12	195	15:29	61.5700	332.1483
H13	195	15:49	61.5967	332.1900
H14	195	20:12	61.1067	333.6350
H15	195	20:33	61.1333	333.6767
H16	196	03:28	61.6250	332.2317
H17	196	03:47	61.6517	332.2717
H18	196	08:07	61.1617	333.7167
H19	196	08:28	61.1883	333.7567
H20	196	13:17	61.6783	332.3133
H21	196	13:36	61.7050	332.3550
H22	196	18:02	61.2150	333.7983
H23	196	18:22	61.2417	333.8383
H24	196	23:27	61.7317	332.3967
H25	196	23:50	61.7550	332.4467
H26	197	04:26	61.2700	333.8917
H27	197	04:47	61.2950	333.9300

H28	197	09:30	61.7800	332.4883
H29	197	09:50	61.8050	332.5283
H30	197	14:27	61.3217	333.9750
H31	197	14:45	61.3467	334.0150
H32	197	19:08	61.8300	332.5683
H33	197	19:28	61.8550	332.6050
H34	197	23:55	61.3717	334.0533
H35	198	00:14	61.3967	334.0900
H36	198	04:34	61.8800	332.6417
H37	198	04:55	61.9050	332.6817
H38	198	09:14	61.4217	334.1283
H39	198	09:32	61.4467	334.1650
H40	198	14:00	61.9300	332.7200
H41	198	14:18	61.9550	332.7583
H42	198	18:43	61.4717	334.2050
H43	198	19:04	61.4950	334.2417
H44	198	23:32	61.9783	332.7967
H45	198	23:50	62.0050	332.8367
H46	199	04:20	61.5217	334.2800
H47	199	04:39	61.5450	334.3183
H48	199	09:00	62.0283	332.8733
H49	199	09:15	62.0500	332.9150
H50	199	13:53	61.5700	334.3583
H51	199	14:20	61.5950	334.3950
H52	199	18:22	62.0750	332.9533
H53	199	18:48	62.1033	332.9983
H54	199	20:32	61.7167	334.1733
H55	199	22:55	61.7467	334.2183
H56	200	03:19	62.1333	333.0450
H57	200	03:42	62.1633	333.0900
H58	200	07:30	61.7767	334.2633
H59	200	07:52	61.8067	334.3100
H60	200	11:24	62.1933	333.1367
	200	11:30		
	200	13:15		
	200	13:27		
	200	14:57		
	200	19:37		
A	201	05:49		
B	201	06:55		
C	201	07:26		
D	201	08:19		

A4. List of XBT and sound velocity probe deployments

No.	Day	Time	Latitude	Longitude	Water depth	No. of Samples	Xducer SV[1]	Comment
0	166	15:52				21		Test
1	166	15:54				11		Test
2	166	16:03				431		Test
3	170	14:44	54.7817	339.4433		11		Failed
4	170	14:50	54.7833	339.4500		141		Failed
5	170	14:58	54.7833	339.5700	2575	1231	1496.6	SVP001
6	171	16:24	57.1800	334.1983	2757	1231	1489.2	
	172	11:55	58.0000	328.5000				SVP002
7	172	15:03	58.0967	328.1250	1299	1231	1481.5	
8	173	15:07	58.4167	327.8000	1691	1231	1481.1	
9	174	15:07	58.6683	328.0467	1407	1231	1479.3	
10	175	15:05	58.6583	328.7550	1497	1231	1483.0	
11	176	15:08	59.5500	329.9717	1136	1071	1484.1	
12	176	15:15	59.5500	329.9717	1136	731	1483.2	
13	178	17:11	58.5317	330.5567	2506	1231	1486.0	
14	179	06:16	58.5900	330.7200	2400	1231	1485.2	)
15	179	07:43	58.7633	330.2717	2029	1231	1483.1	) Traverse
16	179	09:10	58.9350	329.8100	1580	1231	1482.0	) across
17	179	10:39	59.1067	329.3533	1305	51	1483.3	) ridge axis.
18	179	10:52	59.1067	329.3533	1305	1231	1479.6	)
19	179	14:23	59.2950	328.8650	1621	1231	1479.8	SVP003
20	180	15:04	59.3017	329.4033	1338	1231	1482.1	
21	181	15:06	59.2000	330.1333	1570	1231	1486.4	
22	182	15:02	59.1233	330.8033	1775	1231	1488.0	
23	183	15:02	59.5333	329.8367	1220	1231	1484.4	
24	184	15:03	59.6533	330.1917	1047	1231	1486.8	
25	185	15:03	59.9600	330.1683	1275	1231	1485.2	
26	186	15:01	60.2333	330.2367	1562	1231	1486.4	
27	187	15:07	60.3100	330.6383	1206	1231	1487.6	
28	188	15:02	60.5167	330.9617	1074	11		
29	189	16:19	60.3383	332.4017	822	1231	1488.9	
30	190	15:47	60.8367	331.0850	1622	531	1487.4	
31	191	15:04	60.8400	331.8367	1040	1231	1489.0	
32	191	18:01	60.6950	332.2650	1541	521	1489.6	SVP004
33	192	18:18	61.1750	331.9133	964	1231	1487.3	
34	193	15:03	61.2933	332.3550	812			
35	193	15:11	61.2950	332.3550	660			
36	193	15:03	61.2933	332.3550		1231	1488.9	
37	193	15:11	61.2950	332.3550		1231	1489.4	
38	195	16:06	61.5667	332.2833				
39	196	18:53	61.2633	333.7817				
40	197	15:02	61.3800	333.9200				
41	198	15:03	61.8750	332.9950				
42	199	15:13	61.7133	334.0300				

[1] A salinity of 35 ppt is assumed.

A5. Sound velocity profile

These are the sound velocity profiles used to convert travel times to depths for the EM12S-120 during cruise CD87. The profiles were read into the EM12 system immediately after each dip was taken (see appendix A4).

SVP001	54°47.00'N 20°25.83'W	SVP002	58°00.00N 31°30.00'W	SVP003	59°17.40'N 31°09.58'W	SVP004	60°41.68'N 27°44.14'W
depth (m)	sound velocity (m/s)	depth (m)	sound velocity (m/s)	depth (m)	sound velocity (m/s)	depth (m)	sound velocity (m/s)
1	1496.2	3	1483.6	3	1481	2	1490.8
52	1496.7	13	1484.2	40	1481.2	3	1491.1
53	1496.2	42	1484.1	42	1480.6	24	1491.2
66	1495.8	45	1484.6	46	1480.7	32	1491.1
68	1495.2	60	1484.7	51	1480.1	38	1490.2
86	1495.2	63	1484.1	57	1478.7	41	1488.4
87	1494.6	67	1483.9	65	1478.3	43	1487.6
94	1494.6	79	1479.6	70	1479.5	46	1487.4
109	1493.2	81	1479.8	71	1479.1	47	1486.8
118	1493.2	83	1479.2	75	1479.2	49	1486.4
124	1492.4	89	1478.8	76	1478.7	49	1486.1
130	1493.2	102	1478.5	81	1479.1	50	1486.1
133	1492.8	109	1478.9	88	1476.2	53	1485.6
138	1493.2	122	1478.7	93	1475.7	55	1485.6
142	1492.7	130	1479.2	96	1476.2	56	1485.4
161	1492.7	207	1479.1	116	1476.1	58	1484.6
165	1491.1	216	1479.6	120	1476.6	59	1484.4
209	1491.1	245	1479.6	131	1476.8	61	1484.2
210	1490.6	252	1480.2	136	1477.7	64	1484.2
219	1491.1	271	1480.2	142	1477.4	66	1483.6
246	1491.1	274	1480.7	151	1478.7	69	1483.6
253	1490.2	293	1480.6	158	1478.7	71	1483.1
266	1489.6	327	1481.7	167	1479.6	75	1483.1
284	1489.6	339	1481.6	177	1479.1	77	1482.7
292	1490.7	348	1482.1	182	1480.2	81	1482.4
311	1491.6	354	1481.7	203	1480.2	85	1481.7
372	1489.5	359	1482.2	236	1481.2	97	1481.6
397	1489.6	412	1482.1	264	1481.2	99	1481.5
398	1490.2	421	1482.7	274	1481.7	100	1481.1
403	1489.6	461	1482.7	283	1481.7	145	1481.1
408	1489.6	474	1482.1	286	1481.2	146	1481.2
410	1490.2	521	1482.1	308	1481.2	149	1481.7
428	1490.2	524	1482.7	310	1480.6	171	1481.6
430	1489.6	544	1482.5	318	1480.7	199	1481.7
436	1489.6	554	1483.2	323	1480.1	206	1482.2
455	1489.6	580	1483.1	338	1480.7	225	1482.1
459	1490.2	585	1483.6	358	1480.7	244	1482.2
469	1489.6	615	1483.6	374	1480.1	250	1482.7
479	1490.2	621	1484.2	379	1480.6	255	1482.5
485	1489.6	669	1484.2	398	1480.6	257	1482.7
487	1490.3	672	1483.6	404	1481.2	276	1482.7
580	1489.6	684	1484.1	447	1481	285	1483.2
582	1490.2	691	1483.6	459	1481.7	302	1483.1
588	1489.6	757	1483.6	547	1481.6	307	1483.2
595	1489.7	758	1483.1	565	1482.1	312	1483.6
598	1489.2	783	1483.1	569	1481.6	338	1483.6
602	1489.6	785	1482.5	581	1482.2	341	1484
605	1489	825	1482.5	589	1481.7	344	1484.1
618	1489.2	840	1483.2	602	1482.2	351	1484.2
619	1488.6	875	1483.1	613	1482.1	361	1484
630	1488.1	882	1483.6	615	1481.7	364	1484.2
653	1488.8	944	1483.6	618	1482.1	366	1484.1
664	1488.1	949	1484.2	656	1482.1	370	1484.5
697	1488.1	964	1484.1	680	1483.2	374	1484.7
709	1489.7	966	1484.6	730	1483.1	406	1484.6
718	1489.6	977	1484.3	758	1483.6	411	1485.1
723	1490.7	981	1484.7	764	1483.1	433	1485.1
775	1491.3	1025	1484.6	776	1483.3	435	1485.4

786	1490.6	1030	1485.2	781	1482.7	444	1485.7
823	1491.3	1038	1485.2	791	1483.6	460	1485.6
828	1490.2	1046	1484.6	892	1483.6	469	1485.7
853	1490.7	1054	1484.6	897	1484.2	474	1486.1
855	1490	1063	1485.2	930	1484.1	505	1486.1
862	1490	1127	1485	939	1484.6	508	1486.4
865	1490.6	1133	1485.6	944	1484.2	514	1486.7
882	1490.7	1152	1485.8	972	1484.7	526	1486.6
887	1490	1178	1485.6	1013	1484.6	536	1486.7
935	1490.2	1181	1486.1	1018	1485.2	543	1486.5
938	1489.6	1188	1486.1	1056	1485	549	1487.1
970	1489.7	1193	1486.7	1071	1485.7	585	1487.2
992	1489	1214	1486.5	1099	1485.6	591	1487.6
1310	1489.6	1225	1487.1	1110	1486.1	643	1487.6
1317	1490.2	1251	1487.1	1155	1486.1	645	1487.9
1356	1490	1256	1487.7	1163	1486.7	652	1488.2
1374	1490.7	1282	1487.5	1197	1486.5	692	1488.1
1453	1491.1	1290	1488.2	1210	1487.2	693	1488.2
1460	1491.7	1351	1488.6	1235	1487.1	705	1488.1
1491	1491.6	1356	1489.2	1241	1487.7	884	1488.2
1525	1492.7	1386	1489	1267	1487.5	887	1488.1
1563	1492.5	1392	1489.6	1275	1488.2	891	1487.6
1576	1493.2	1418	1489.6	1302	1488.1	935	1487.6
1604	1493.1	1422	1490.2	1307	1488.6	939	1488.2
1611	1493.7	1451	1490.2	1356	1489	960	1488.1
1615	1493.1	1455	1490.7	1368	1489.7	975	1488.2
1640	1493.8	1482	1490.6	1425	1490	982	1488.1
1665	1493.7	1489	1491.1	1436	1490.7	986	1487.6
1695	1494.8	1518	1491.1	1459	1490.6	1000	1487.5
1714	1494.6	1523	1491.7	1468	1491.1	1016	1487.6
1718	1495.2	1548	1491.6	1491	1491.1	1021	1488.1
1751	1495.1	1556	1492.2	1498	1491.7	1029	1488.2
1759	1495.8	1576	1492.1	1515	1491.6	1048	1488.1
1830	1496.7	1585	1492.7	1527	1492.2	1091	1488.2
1857	1496.6	1603	1492.5	1547	1492.1	1098	1488.1
1869	1497.3	1615	1493.2	1552	1492.7	1099	1488.2
		1638	1493.2	1606	1493.2	1101	1488.1

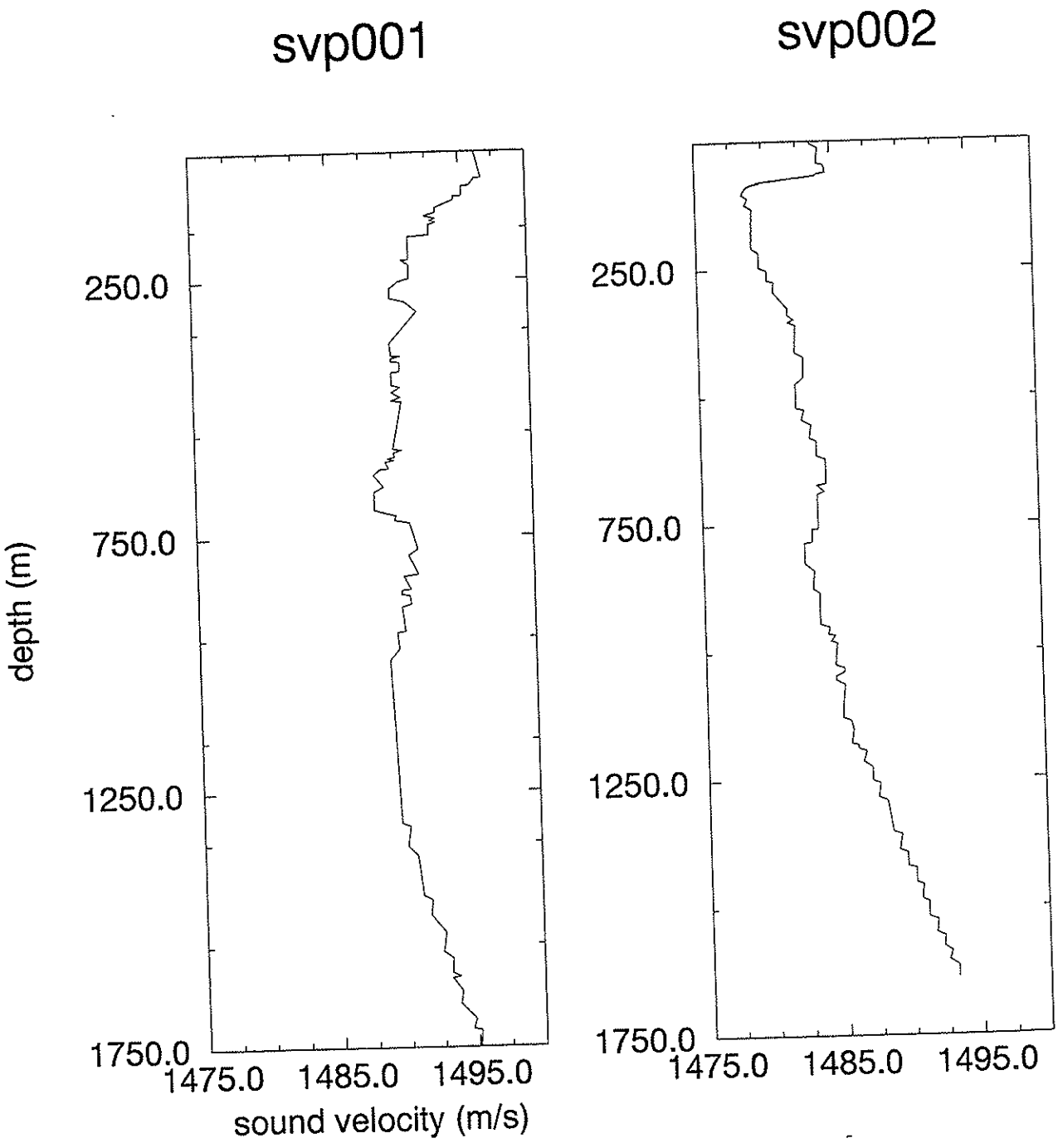
svp001
svp002
depth (m)
250.0
750.0
1250.0
1750.0
1475.0
1485.0
1495.0
sound velocity (m/s)

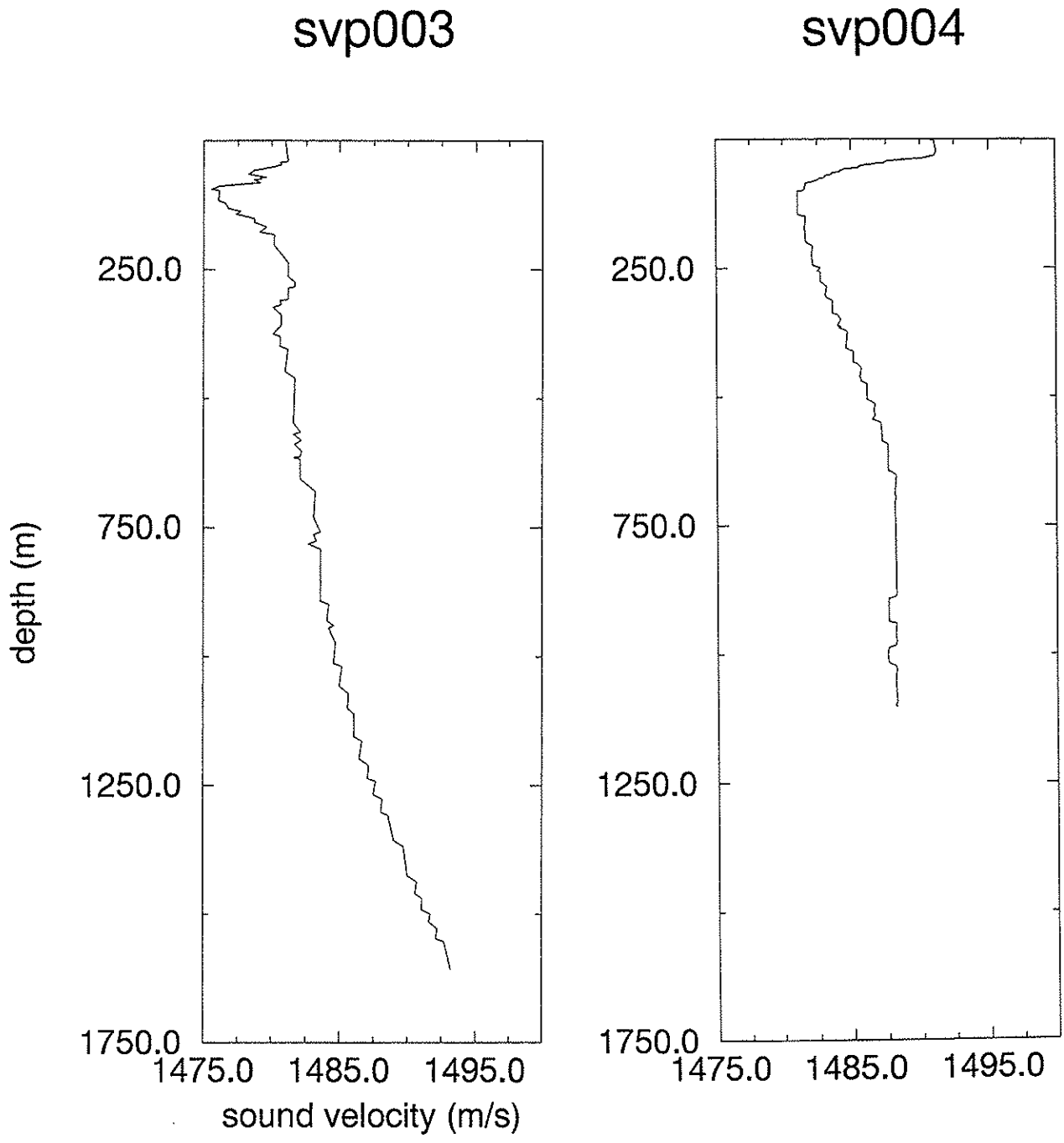
svp003
svp004
depth (m)
250.0
750.0
1250.0
1750.0
1475.0
1485.0
1495.0
sound velocity (m/s)

A6. References

Angenheister, G., S. Bjornsson, P. Einarsson, H. Gebrande, P. Goldflam, W.R. Jacoby, I.V. Litvinenko, B. Loncarevic, H. Miller, G. Palmason, N.I. Pavlenkova, S. Richard, S.C. Solomon, W. Weigel and S.M. Zverev, 1980. Reykjanes Ridge Iceland Seismic Experiment (RRISP 77). J. Geophysics 47, 228-238.

Appelgate, B., and Shor, A.N., 1994. The northern mid-Alantic and Reykjanes Ridge - spreading center morphology between 55°50'N and 63°00'N, Journal of Geophysical Research 99, 17935-17956.

Bell, R. E., and Buck, W. R., 1992. Crustal control of ridge segmentation inferred from observations of the Reykjanes Ridge. Nature, 357, 583-586.

Blondel, P. & Parson, L.M., 1994. Sonar processing in the UK - a short review of existing potential and new developments for the BRIDGE community, BRIDGE report.

Brozena, J.M. & White, R.S., 1990. Ridge jumps and propagations in the South Atlantic Ocean. Nature, 348, 149-152.

Bunch, A.W.H. and B.L.N. Kennett, 1980. The crustal structure of the Reykjanes Ridge at 59° 30'N. Geophys. J. Roy. astr. Soc., 61, 141-166.

Caress, D.W., and Chayes, D.N., MB-System manual pages.

Courtney, R. C., and White, R. S., 1986. Anomalous heatflow and geoid across the Cape Verde Rise: evidence for dynamic support from a thermal plume in the mantle. Geophysical J. R. astr. Soc., 87, 815-868.

DeMets, C., Gordon, R.G., Argus, D.F. & Stein, S.,1989. Current Plate Motions. Geophysical Journal Int., 101, 425-478.

de Moustier, C., & Kleinrock, M.C., 1986. Bathymetric artifacts in Sea Beam data: how to recognize them and what causes them. Journal of Geophysical Research 91, 3407-3424.

German, C.R., Briem, J., Chin, C., Danielson, M., Holland, S., James, R., Jónsdóttir, A., Ludford, E., Moser, C., Ólafsson, J., Palmer, M., and Rudnicki, M., 1993. Hydrothermal activity on the Reykjanes Ridge: the Steinahóll vent field at 63°06'N, BRIDGE News 5, 18-19.

Goldflam, P., W. Weigel and B.D. Loncarevic, 1980. Seismic structure along RRISP - profile 1 on the southeast falnk of the Reykjanes Ridge. J. Geophysics, 47, 250-260.

Jacoby, W. R., 1980. Morphology of the Reykjanes Ridge Crest Near 62ºN. J. Geophys., 47, 81-85.

Haxby, W.F., 1987, Gravity Fields of the World's Oceans: National Geophysical Data Center, Boulder, Co.

Hwang, L., Parsons, B., Strange, T., and Bingham, A., 1994. A detailed gravity field over the Reykjanes Ridge from Seasat, Geosat, ERS-1 and TOPEX/POSEIDON altimeter data and shipborne gravity data, Geophysical Research Letters, (in press).

Keeton, J.A., & Mitchell, N.C., 1994. The interpretation of multibeam images. BRIDGE News 6.

Kuo, BY & DW Forsyth, 1988. Gravity anomalies of ridge-transform system in South Atlantic. Mar. Geophys. Res., 10, 205-232.

Kuznetsov, A. P., Bogdanov, YU. A., Sagalevich, I. M., Sboshikov, A. M., Almukamedov, M. I., Podrazhansky, A. M., & Gorlov, A. A., 1985. Geological investigations of Reykjanes Ridge from submersibles. Oceanology, 25, 77-82.

Lin, J., Purdy, G. M., Schouten, H.,& Sempere, J.-C.,& Zervas, C.,1990. Evidence from gravity data for focussed magmatic accretion along the Mid-Atlantic Ridge. Nature, 344, 627-632.

McKenzie, D. P., & M. J. Bickle, 1988. The volume and composition of melt generated by extension of the lithosphere. J. Petrol., 29, 625-679.

Murton, B. J., and Parson, L. M., 1993. Segmentation, volcanism and deformation of oblique spreading centres - a quantitative study of the Reykjanes Ridge, Tectonophysics 222, 237-257.

Murton, B. J., Evans, J., Forster, J., Owens, R., Parson, L.M., Redbourne, L., Sauter, D., Slater, L., Taylor, R.N., and Walker, C.L., 1993. The PETROS programme: a report from CD80, BRIDGE News 5, 22-26.

Olafsson, J. Thors, K., and Cann, J., 1991. A sudden cruise off Iceland. RIDGE Events, 2, p. 35

Owens, R. 1994, The MB-system software for the manipulation and display of multibeam bathymetry data. BRIDGE News 6.

Owens, R. B., Searle, R. C., Field, P., Parson, L. M., and Spencer, S. , 1991. The first non-transform offset on the Reykyanes Ridge. EOS, Trans. Amer. Geophys. Union, 72, 467.

Parker, R.L., and Huestis, S.P., 1974. The inversion of magnetic anomalies in the presence of topography, J. Geophys. Res. 79, 1587-1593.

Parmentier, E. M., & Phipps Morgan, J., 1990. Spreading rate dependence of three-dimensional structure in oceanic spreading centres. Nature, 348, 325-328.

Parson, L. M., Murton, B. J., Searle, R. C., Booth, D., Evans, J., Field, P., Keeton. J., Laughton, A., McAllister, E., Millard, N., Redbourne, L., Rouse, I., Shor, A., Smith, D., Spencer, S., Summerhayes, C., and Walker, C., 1993. En echelon axial volcanic ridges at the Reykjanes Ridge: a life cycle of volcanism and tectonics. Earth Planet. Sci. Lett. 117, 73-87.

Ritzert, M. and W.R. Jacoby, 1985. On the Lithospheric Seismic Structure of the Reykjanes Ridge at 62.5oN. J. Geophys. Res., 90, 10117-10128.

Schilling, J.-G., Zajac, M., Evans, R., Johnston, T., White, W., Devine, J. D., and Kingsley, R., 1983. Petrologic and geochemical variations along the Mid-Atlantic Ridge from 29°N to 73°N. Amer. J. Science, 283, 510-586.

Scott, D. R., and Stevenson, D. J., 1986. Magma ascent and porous flow. J. Geophys. Res., 91, 9283-9296.

Searle, R. C. & Laughton, A. S., 1981. 1981. Fine-scale sonar study of tectonics and volcanism on the Reykjanes Ridge. Ocean. Acta, suppl. to v. 4, 5-13.

Searle, R. C., Field, P., Owens, R. B., and Parson, L. M., 1992a. A non-transform ridge offset on the Reykyanes Ridge. Annales Geophysicae, suppl. to v. 10, C66.

Searle, R. C., Field, P., and Owens, R. B., 1994. Segmentation and a non-transform spreading offset on the Reykyanes Ridge, Journal of Geophysical Research 99, 24159-24172.

Simrad 1992, SIMRAD EM12 hydrographic echo sounder, product description: Simrad Subsea A/S, Horten, Norway, #P2302E.

Snoek, M. and S. Goldflam, 1978. Crustal structure of the Reykjanes Ridge at 63°N derived from refraction seismic measurements. J. Geophys., 45, 107-109.

Strange, T., 1991. The determination and geophysical applications of free air gravity anomalies using satellite altimetry and ship gravity. PhD thesis, University of Oxford.

Talwani, M., C.C. Windisch and M.G. Langseth, 1971. Reykjanes Ridge Crest: A Detailed Geophysical Study. J. Geophys. Res., 76, 473-577.

Vogt, P.R., 1971. Asthenosphere motion recorded by the ocean floor south of Iceland. Earth Planet. Sci. Lett., 13, 153-160.

Vogt, P.R. and O.E. Avery, 1974. Detailed magnetic surveys in the northeast Atlantic and Labrador Sea. J. Geophys. Res., 79, 363-389.

Vogt, P. R., & Johnson, G. L., 1975. Transform faults and longitudinal flow below the midoceanic ridge. J. Geophys., Res., 80, 1399-1428.

Watson, S. P., & McKenzie, D. P., 1991. Melt generation by plumes: a study of Hawaiian volcanism. J. Petrology, 32, 501-537.

Wessel, P., & Smith, W.H.F., 1991. Free software helps map and display data. EOS Trans. AGU, 72, 441, 445-446.

White, R. S., 1992a. Melt production rates in mantle plumes. Phil. Trans. Roy. Soc. London, A, in press.

White, R. S., 1992b. Crustal structure and magmatism of North Atlantic continental margins. J. Geol. Soc. London, 149, 841-854.

White, R. S., 1992c. Seismic surveys in the Atlantic. BRIDGE News, 3, 30-31.

White, R. S., McKenzie, D. P., and O'Nions, R. K., 1992. Oceanic crustal thickness from seismic measurements and rare earth element inversions, Journal of Geophysical Research 97, 19683-19713.